GDCh

**Research Articles**

*Angewandte*
*Chemie*
International Edition
www.angewandte.org

**Protein Engineering**

# Tumor-Cell-Specific Targeting of Ibrutinib: Introducing Electrostatic Antibody-Inhibitor Conjugates (AiCs)

*Andreas Faust+, Nicole Bäumer+, Alina Schlütermann, Manuel Becht, Lilo Greune, Christiane Geyer, Christian Rüter, Renato Margeta, Lisa Wittmann, Petra Dersch, Georg Lenz, Wolfgang E. Berdel, and Sebastian Bäumer\**

**Abstract:** *Ibrutinib is an inhibitor of Bruton's tyrosine kinase that has been approved for the treatment of patients with chronic lymphocytic leukemia, mantle cell lymphoma and Waldenstrom's macroglobulinemia and is connected with toxicities. To minimize its toxicities, we linked ibrutinib to a cell-targeted, internalizing antibody. To this end, we synthesized a poly-anionic derivate, ibrutinib-Cy3.5, that retains full functionality. This anionic inhibitor is complexed by our anti-CD20-protamine targeting conjugate and free protamine, and thereby spontaneously assembles into an electrostatically stabilized vesicular nanocarrier. The complexation led to an accumulation of the drug driven by the CD20 antigen internalization to the intended cells and an amplification of its pharmacological effectivity. In vivo, we observed a significant enrichment of the drug in xenograft lymphoma tumors in immune-compromised mice and a significantly better response to lower doses compared to the original drug.*

## Introduction

In the last decades, efforts in the analysis of cancer-driving molecular pathways have led to significant progress in the development of specific therapies.[1] The emerging techniques, that is, the identification of tumor specific mutations, production of antibodies and screening methods to identify inhibiting agents were combined and tested in a plethora of clinical studies. However, cancer is still a harmful disease and a leading cause of death worldwide.

Usually, antibody-drug-conjugates (ADC) consist of an antibody, a cytotoxic molecule and a linker. The cell-type specific antibody provokes internalisation into the cancer cell,

next a rather unspecific but efficient cytotoxic molecule kills the cells as soon as it is internalized.[2,3] The chemical linker between antibody and cytotoxic molecule is either intracellularly cleavable, that is, at lower pH values within the endosomal vesicle, or uncleavable to prevent early liberation of the dangerous cytotoxic molecule.[4] This concept has several advantages such as more cell-type specific targeting. However, in the last 20 years less than 10 ADCs were FDA-approved.[2,3] One example is gemtuzumab-ozogamicin (GO, Mylotarg^R), which is composed of the anti-CD33-antibody gemtuzumab that mainly targets myeloid cells that is, in acute myeloid leukemia, linked to the cytotoxic ozogamicin.[5] FDA-approved in 2000, GO was withdrawn 2010 due to high side effects and low survival advantages, which possibly was explainable by the leakiness of the cleavable hydrazone linker.[4] With modified doses and application, GO was reapproved by the FDA in 2017. Problems with this and other ADCs are: Lack of internalization efficiency of the antibody demands higher doses, lack of specificity of the cytotoxic molecules leads to spill-over and side-effects, and various ways for the cancer cell to acquire resistance, especially when the doses have to be lowered due to toxicity.

Ibrutinib as a small molecule inhibitor significantly improved treatment of patients with mantle cell lymphoma and chronic lymphocytic leukemia.[6] Ibrutinib is an orally available covalent inhibitor of the Bruton's tyrosine kinase (BTK) binding at cysteine 481.[7] This leads to an irreversible inhibition of the autophosphorylation site and downstream signaling cascade. Since the respective cells are dependent on this signaling, ibrutinib treatment leads to effective growth inhibition and induction of apoptosis, depending on cell-

[*] A. Faust,[+] R. Margeta
European Institute for Molecular Imaging, University of Münster
Waldeyerstr. 15, 48159, Münster (Germany)

N. Bäumer,[+] A. Schlütermann, M. Becht, L. Wittmann, G. Lenz, W. E. Berdel, S. Bäumer
Department of Medicine A, Hematology/Oncology, University Hospital Münster
Albert-Schweitzer Campus 1, 48149 Muenster (Germany)
E-mail: baumers@uni-muenster.de

L. Greune, C. Rüter, P. Dersch
Institute for Infectiology, Center for Molecular Biology of Inflammation (ZMBE), University of Münster
Von-Esmarch-Str. 56, 48149 Münster (Germany)

C. Geyer
Institute for Clinical Radiology, University Hospital Münster
Albert-Schweitzer Campus 1, 48149 Münster (Germany)

A. Faust,[+] N. Bäumer,[+] S. Bäumer
Interdisciplinary Center of Clinical Research (IZKF), University of Münster
Albert-Schweitzer Campus 1, 48149 Münster (Germany)

[+] These authors contributed equally to this work.

Supporting information and the ORCID identification number(s) for the author(s) of this article can be found under:
https://doi.org/10.1002/anie.202109769.

intrinsic determinants.[8] However, also the application of untargeted ibrutinib can provoke side effects[7] and can lead to acquired resistance mechanisms.[9] To combine both targeted therapy agents, we based our approach on an antibody-conjugation strategy that we initially generated to target siRNA via antibodies into a tumor cell.[10] Accordingly, we conjugated the anti-CD20 monoclonal antibody (mAB, α) rituximab via the linker sulfo-SMCC to the cationic peptide protamine and simultaneously exploited free protamine. Binding of an anionic partner molecule and formation of a conjugate occurs by electrostatic binding, and we therefore needed an appropriate anionic small molecule partner. Hence, we designed and synthesized an anionic ibrutinib by adding the fluorescent marker Cy3.5™ representing anionic charges in one site of the molecule and offering also a fluorescence readout for analysis.

Here, we present data about the synthesis, binding capacity, specificity, and efficacy of this antibody-inhibitor conjugate in form of an electrostatic nanocarrier in models of diffuse large B-cell lymphoma (DLBCL). DLBCL represents the most frequent lymphoma subtype in adults.[11] The introduction of rituximab has made significant impact on the outcome of DLBCL patients. The combination of rituximab and cyclophosphamide, doxorubicin, vincristine, and prednisone (CHOP) represents the standard first-line therapy in the vast majority of patients. However, patients who are refractory to first-line treatment or relapsing after initial response are characterized by poor survival,[7] indicating that novel therapeutic approaches are urgently needed. Ibrutinib targets B-cell receptor (BCR) signaling that is critical for survival of subsets of DLBCL. As a drawback, the ATP-pocket target cysteine residue is conserved among nine other tyrosine kinases.[12,13] These processes lead to higher dosage of ibrutinib, its interception by irrelevant cells and in addition even to adverse effects, which could be partly due to the bystander effects on targets other than BTK.[14] Next, prolonged ibrutinib dosage can lead to development of resistance.[9]

## Results and Discussion

To circumvent some of the disadvantages discussed above, we intended to construct a conjugate that consists of a tumor-targeting antibody and an inhibitor of a tumor-driving kinase, which confers double specificity and therefore safer application, and which assembles only by electrostatic interaction. As an example, we chose the B-cell specific anti-CD20 antibody rituximab[15] and the B-cell pathway inhibitor ibrutinib,[14,16] mainly because both are part of standard therapies.

First, we converted the uncharged ibrutinib to the strongly anionic compound ibrutinib-Cy3.5, which allowed to bind by means of electrostatic force to our cationic protamine-based carrier system to form an antibody-inhibitor-complex (Scheme 1 A). The cyanine dye Cy3.5 exhibits strong anionic character by exposing four sulfonic acid groups as potential electrostatic binders. It is important to concentrate the anionic charges on one site of the molecule and to retain an overall linear shape to form the nanocarrier. In addition, the

cyanine dye allows a fluorescence read out in all stages of evaluation. According to the literature,[17] we synthesized a protected amino-functionalized ibrutinib-derivative **9** starting with the commercially available pyrazolopyrimidine which was subsequently iodinated and substituted with 4-phenyloxy-benzene boronic acid via Suzuki-coupling to form the main part **2** of the ibrutinib core structure. To receive high binding affinity (S)-N-Boc-3-hydroxypiperidine was installed via Mitsunobu reaction forming compound **4**. After deprotection of the piperidine moiety an α,β-unsaturated linker **7** (Michael acceptor) was introduced for irreversible binding to the target.[18] The resulting Boc-protected amine **9** represents the lead structure for labelling with the cyanine dye Cy3.5 yielding ibrutinib-Cy3.5 (Scheme 1 A). Ibrutinib-Cy3.5 was then incorporated into the electrostatic nanocarrier (Scheme 1 B).

Besides the strong polyanionic character of the Cy3.5 dye, the conjugate had the advantage of being easily traceable *in vitro* and *in vivo* in form of a red fluorescence (Figure 1).

For the formation of the carrier monoclonal antibody, αCD20-mAB was conjugated to SMCC-protamine by cysteines of the IgG backbone (Scheme 1 B). The conjugation was observable by molecular weight shifts in the IgG heavy chain as well as the light chain, indicating the binding of one protamine peptide per light and heavy chain of the IgG (Figure 1 A). The resulting αCD20-mAB-protamine conjugate was successfully tested for CD20-receptor binding and internalization by flow cytometry analysis (Support. Figure 2 A). To form a carrier conjugate suitable to complex ibrutinib-Cy3.5 efficiently, a certain molar excess of free non-bound SMCC-protamine over the carrier αCD20-mAB-P is necessary, here, a 32:1 molar ratio was shown to be optimal in terms of stable complexation of ibrutinib-Cy3.5 (Figure 1 B, Support. Figure 2 B). In these assays, αCD20-mAB-protamine/free protamine (αCD20-mAB-P/P) complex allowed to bind more than 100 mol ibrutinib-Cy3.5 per mol of carrier antibody by means of electrostatic force to our protamine-based carrier system. This carrier assembly depends on the presence of an excess of free (SMCC-)protamine, as depletion of free SMCC-protamine leads to non-assembly or destruction of the carrier (Support. Figure 3). We therefore conclude that free protamine is essential for nanocarrier formation, which we now call αCD20-mAB-P/P-ibrutinib-Cy3.5 to indicate this composition.

The building of an antibody-inhibitor-complex in form of stable nanoparticles could be detected in fluorescence microscopy (Figure 1 C–H), which are stable in serum (Figure 1 E–H) under conditions as published for other nanoparticles.[19] Importantly, as ibrutinib-Cy3.5 is detectable by fluorescence, this brings along excellent tracing abilities for all downstream applications.

When incubated *in vitro*, αCD20-mAB-P/P loaded with ibrutinib-Cy3.5 led to the assembly of electrostatically stabilized nanoparticles exposing red Cy3.5 fluorescence (Figure 2). In fluorescence microscopy, first regular shaped vesicular structures (Figure 1 C,D), later irregular shaped aggregates larger than 2 μm plus smaller particles were detected, this process was not seen, if unmodified αCD20-mAB was used to complex ibrutinib-Cy3.5, or modified
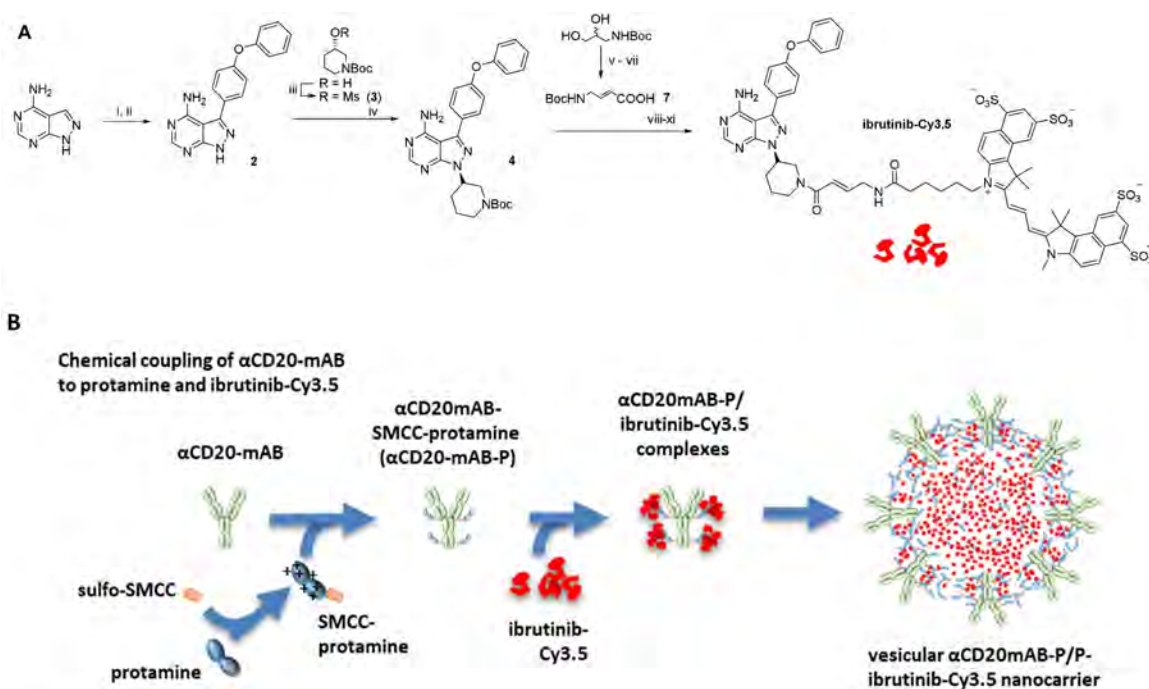
**Scheme 1.** Synthesis of ibrutinib-Cy3.5 and the vesicular αCD20-mAB-P/free P-ibrutinib-Cy3.5 nanocarrier. **A:** Synthesis of ibrutinib-Cy3.5: (i) NIS, DMF, 80°C; (ii) p-phenoxyphenylboronic acid, Pd(PPh$_3$)$_4$, KOH, dioxane/water 5:1, MW, 180°C, 10 min, 58% (two steps); (iii) MeSO$_2$Cl, Et$_3$N, DCM, rt, 77%; (iv) K$_2$CO$_3$, DMF, 80°C, overnight, 46%; (v) NaIO$_4$, H$_2$O, rt, 84%; (vi) (EtO)$_2$P=OCH$_2$COOEt, NaH, THF, 0°C to rt, 35%; (vii) LiOH, THF/H$_2$O 2:1, rt, 83%; (viii) 4 M HCl$_{(g)}$/dioxane, EtOAc/MeOH 1:1, rt, 98%; (ix) **7**, PyAOP, DIPEA, MeCN, 72%; (x) 4 M HCl$_{(g)}$/dioxane, EtOAc/MeOH 1:1, rt; (xi) sulfo-Cy3.5 NHS ester, DIPEA, DMF, rt, 80%, two steps. **B:** Schematic overview: the αCD20-mAB was conjugated to SMCC-protamine via cysteine sulfhydryls (SMCC) to obtain αCD20-mAB-protamine (αCD20-mAB-P) and then in the presence of additional free protamine anionic ibrutinib-Cy3.5 electrostatically binds to the cationic protamines forming the vesicular αCD20-mAB-P/free P-ibrutinib-Cy3.5 nanocarrier.

αCD20-mAB-P/free protamine was used to complex hydrophobic ibrutinib (Imbruvica$^R$) (not shown). The electrostatic particles seen in light microscopy (Figure 2 A,B) were also validated in electron microscopy (Figure 2 C), where a multitude of smaller particles ranging < 100–200 nm were detected (Figure 2 C), which induced us to choose the term "nano"-carrier.

Next, we investigated the efficacy of this αCD20-mAB-P/P-ibrutinib-Cy3.5 nanocarrier in different cellular model systems.

First, we examined the internalisation into CD20-positive DLBCL cells via Cy3.5 fluorescence. HBL1 and TMD8 lymphoma cells treated overnight with uncoupled ibrutinib-Cy3.5 show decent red fluorescence marking of cells (Figure 3 E and Support. Figure 4 E), which was intensified, when ibrutinib-Cy3.5 was complexed and transported with αCD20-mAB-P/P (Figure 3 F and Support. Figure 4 F). This indicated a beneficial process of internalization by the CD20 receptor over the untargeted uptake mechanisms for ibrutinib-Cy3.5 anion without carrier antibody implementation (Figure 3 E compared to 3 F). Next, a 72 hrs treatment of cells with the conjugates show a singular band of covalent Cy3.5 marking of a 70 kDa protein in an SDS PAGE electrophoresis, indicating binding and functionality of the modified ibrutinib-Cy3.5 compound (Figure 3 G; see Support. Figure 4 G and H for 24 h and 48 h treatment). For fluorescence detection of BTK, the gel had to be considerably overloaded, in order to show

equal loading of lanes and identification of BTK, so next we blotted the gel for immunodetection of BTK after fluorescence detection. Indeed, a band representing BTK appeared at the same position as seen in the Cy3.5 fluorescence, indicating that ibrutinib-Cy3.5 had covalently bound exclusively to BTK, as anticipated (Figure 3 G; see Support. Figure 4 G,H).

Moreover, HBL1 cells were incubated with ibrutinib-bodipy for 2 h, washed and treated with αCD20-mAB-P/P-ibrutinib-Cy3.5. Cells incorporate ibrutinib-bodipy (Figure 3 N,P), but Cy3.5 fluorescence only appears in non-pretreated cells (Figure 3 L) and not in cells pre-treated with ibrutinib-bodipy (Figure 3 P). Some subcellular red vesicles indicate CD20-mediated internalization of ibrutinib-Cy3.5 (Figure 3 P), but a pattern that hints at BTK binding (see Figure 3 L for ibrutinib-Cy3.5 and Figure 3 N,P for ibrutinib-bodipy) does not occur. This is also true after 24 h of αCD20-mAB-P/P-ibrutinib-Cy3.5 treatment (Support. Figure 5) and after pre-incubation with and washout of non-fluorescent ibrutinib (Support. Figure 6).

The functional effect of covalent targeting of BTK by ibrutinib is the inhibition of BTK autophosphorylation ability.[14] Therefore, we analysed the phosphorylation status of BTK in DLBCL cells after ibrutinib-Cy3.5 treatment with and without complexation in the nanocarrier (Figure 4 A and Support. Figure 7 A). Cells were treated for 72 hrs with PBS, uncomplexed ibrutinib-Cy3.5 and with the αCD20-mAB-P/P-
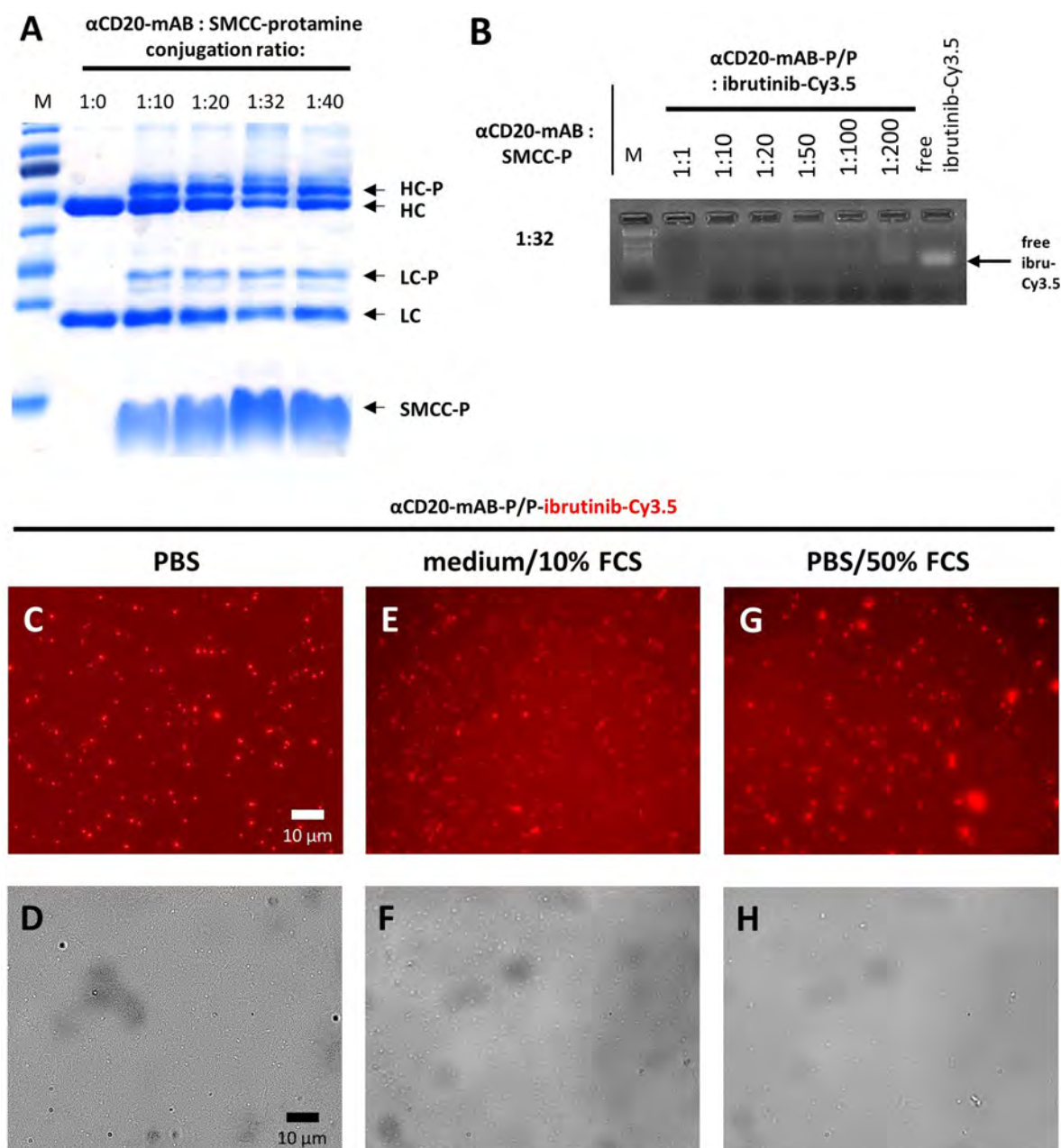
**Figure 1.** Properties of the αCD20-mAB-protamine-ibrutinib-Cy3.5/free P nanocarrier. **A:** SDS-PAGE illustrating molecular weight shifts by protamine conjugation of heavy chain (HC to HC-P) and light chain (LC to LC-P) of αCD20-mAB conjugated to rising amounts of SMCC-protamine. **B:** electromobility shift assays showing the electrostatic loading capacity of ibrutinib-Cy3.5 to conjugates from A. The conjugation ratio of 1:32 was optimal in terms of loading capacity of more than 100 mol ibrutinib-Cy3.5 per mol of αCD20-mAB-protamine. **C–H:** Stability after 1 h-auto-assembly of αCD20-mAB-protamine, free protamine and ibrutinib-Cy3.5 in a 1:20 ratio and subsequent incubation for 24 h in PBS (C, D), and in challenging conditions such as cell culture medium RPMI/10% FCS (E, F) and PBS/50% FCS (G, H). C, E, G, Cy3.5 fluorescence, D, F, H, phase contrast. α, anti; FCS, fetal calf serum.

ibrutinib-Cy3.5 complex, lysed and subjected to Western blot analysis. We found that phosphorylation of BTK at tyrosine 223, detected by a specific phospho-BTK-antibody was significantly decreased in HBL1 (Figure 4 A, left panel) and TMD8 cells (Support. Figure 7 A, right panel) upon treatment with ibrutinib-Cy3.5, irrespective if it was complexed or not. This was in accordance with its binding to BTK as depicted in Figure 3 G. Expression of total BTK was mildly influenced (Figure 4 A and Support. Figure 7 A). We concluded that the synthesized ibrutinib-Cy3.5 conjugate retains full functionality in terms of binding the target molecule BTK as well as inactivation of BTK autophosphorylation.

Interestingly, in all tested lymphoma cell lines, the lymphoma-specific αCD20-mAB-P/P-ibru-Cy3.5 nanocarrier system significantly inhibited colony growth in soft agar cultures. This was observed to a much lower degree for ibrutinib or ibrutinib-Cy3.5 as single agents, and not if unmodified rituximab (αCD20-mAB) was used (HBL1: Fig-
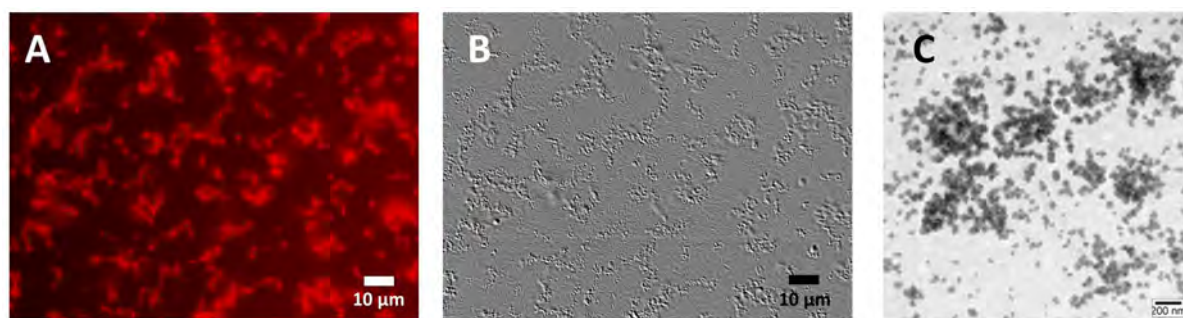
**Figure 2.** Electrostatic nanoparticle formation by αCD20-mAB-protamine/free protamine-ibrutinib-Cy3.5. The carrier antibody-protamine conjugate was loaded with anionic ibrutinib-Cy3.5 in 1:20 ratio and applied to cell-culture treated glass slides for fluorescence microscopy (**A, B**) or copper grids for phospho-Wolfram negative stained electron microscopy (**C**). Here, the electrostatic loading led to the formation of numerous aggregates, where the larger aggregates showed intense Cy3.5 fluorescence (A) and were visible in light microscopy using emboss dynamic filter to illustrate 3D structures through contrast enhancement (B). In transmission electron microscopy (C), negative staining led to roughly the same range of particle sizes but revealed the presence of a plethora of smaller vesicles (C) undetectable in light microscopy. α, anti.
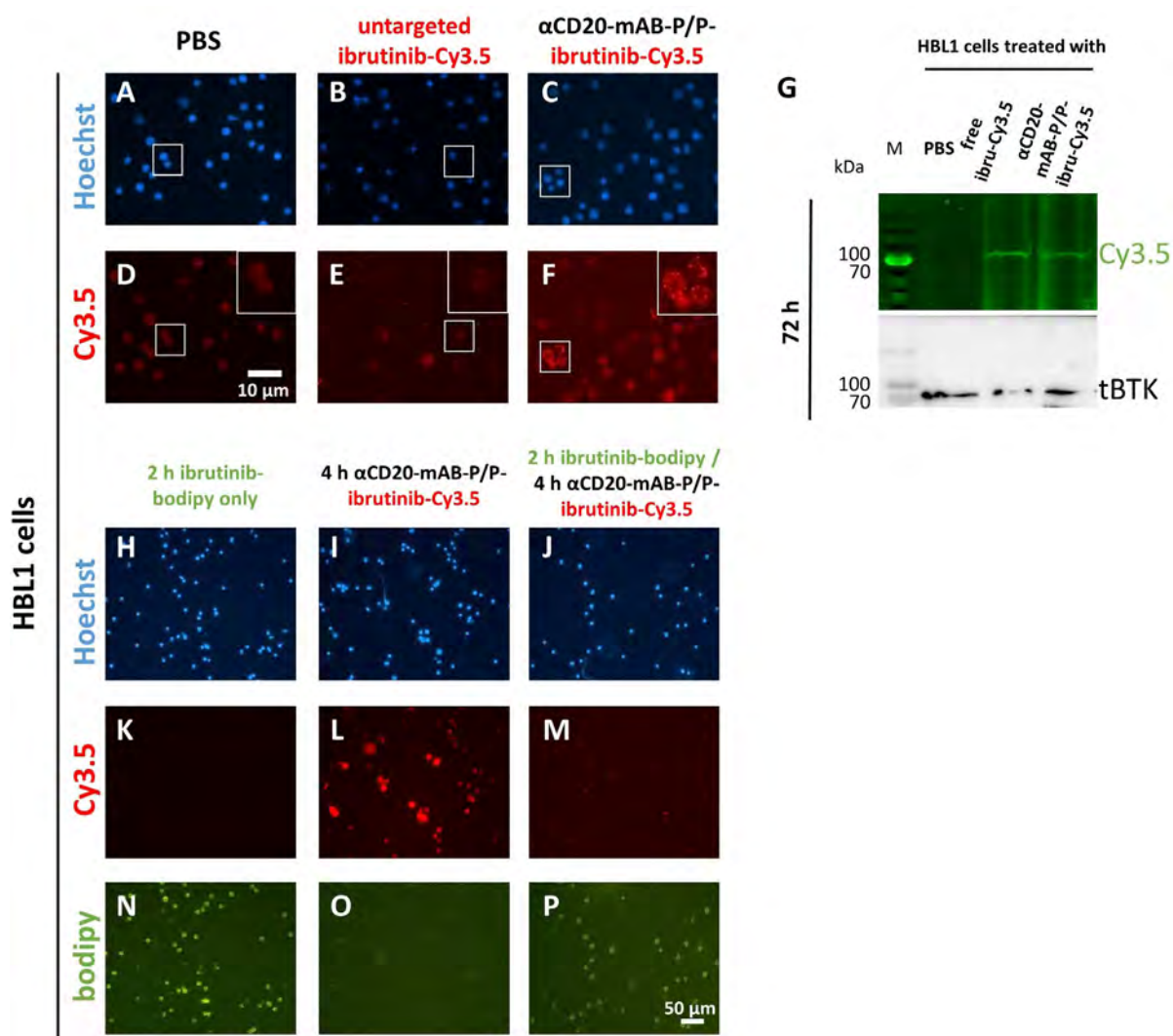


**Figure 3.** Cellular targeting of Bruton's kinase BTK by αCD20-mAB-P/P-complexed ibrutinib-Cy3.5. **A–F:** fluorescence microscopy of HBL1 DLBCL cells treated with targeting conjugates and controls showing a marked intracellular enrichment of Cy3.5-signals. **G:** lysates from cell treated for 72 h with targeting conjugates and controls were subjected to SDS PAGE and illuminated for Cy3.5 signals. Here a clear band of 70 kDa, identified as BTK by parallel immunoblot, was covalently marked by ibrutinib-Cy3.5, indicating binding and thus functionality of the ibrutinib-Cy3.5 derivate. **H–P:** fluorescence microscopy of HBL1 DLBCL cells pre-treated with ibrutinib-bodipy (green, N and P) do not show intracellular enrichment of Cy3.5-signals after αCD20-mAB-P/P-ibrutinib-Cy3.5 treatment (M, compared to L). α, anti.
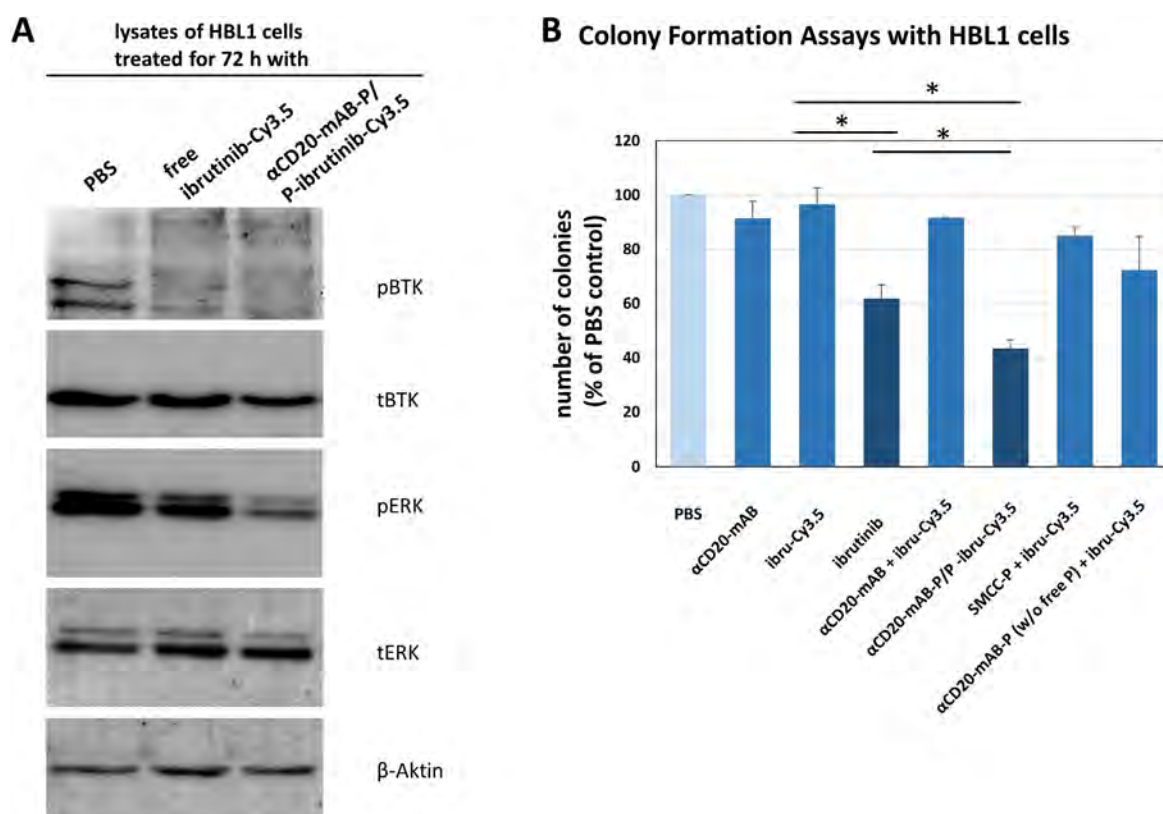
**Figure 4.** Physiological and functional consequences of BTK-inactivation by αCD20-mAB-protamine/free protamine-ibrutinib-Cy3.5 treatment in DLBCL cell lines. **A:** HBL1 cells were treated by the respective conjugates shown for 72 hrs, lysed and subjected to SDS-PAGE and Western blotting for phospho-BTK (pBTK), total BTK (tBTK), phospho-ERK (p-ERK), total-ERK (t-ERK) and actin as a loading control. Here, untargeted ibrutinib-Cy3.5 inhibited the phosphorylation of BTK a bit less than αCD20-mAB-P/P-ibrutinib-Cy3.5, the difference of expected downstream phosphorylation targets such as ERK was more pronounced: Here, only αCD20-mAB-P/P-ibrutinib-Cy3.5 treatment was able to reduce ERK phosphorylation. **B:** In colony formation assays, untargeted ibrutinib-Cy3.5 modestly reduced colony growth of HBL1 cells, while the specific targeting of ibrutinib-Cy3.5 by αCD20-mAB-P/P boosted the colony growth reduction to below 50 %. In order to demonstrate the significance of the free protamine in the conjugate construct, we depleted it from the conjugate mixture, the application of this combination revealed no more colony forming reduction than the single application of ibrutinib-Cy3.5, so the antibody conjugate has lost its targeting ability (B, rightmost bar). α, anti.

ure 4B, and TMD8: Support. Figure 7B). This colony-assay is used for quantification of anchorage-independent clonal cell growth and is a standard *in vitro* surrogate for tumorigenicity *in vivo*. We therefore argue that a robust therapeutic effect of ibrutinib-Cy3.5 is only seen, when the anionic compound is assembled into a stable electrostatic nanoparticle composed of the cationic αCD20-mAB-protamine/free protamine carrier complex and the anionic cargo effector.

Next, we explored the functional consequences of BTK inactivation by αCD20-mAB-P/P-ibrutinib-Cy3.5 on DLBCL cell lines in terms of induction of apoptosis. Here, in HBL1 (Figure 5) as well as in TMD8 cells (Support. Figure 8), αCD20-mAB-P/P-ibrutinib-Cy3.5 treatment offered superior induction of apoptosis signals (Figure 5 and Support. Figure 8, rightmost bars, respectively), whereas the uncomplexed ibrutinib-Cy3.5 treatment showed only mild effects in comparison to the targeted treatment as well as the free ibrutinib treatment. We therefore argue that the targeted treatment of αCD20-mAB-P/P-ibrutinib-Cy3.5 leads to an accumulation of active ibrutinib-Cy3.5 in the cells and hence to a more severe induction of apoptosis than the uncomplexed ibruti-

nib-Cy3.5. It also seems that the anionic molecule ibrutinib-Cy3.5, if uncomplexed is less accessible or at least less effective to the cells as the hydrophobic free ibrutinib, judged by the lower induction of apoptosis as compared to free ibrutinib.

For an *in vivo* application, ibrutinib-Cy3.5 had an additional advantage over free ibrutinib: In contrast to the hydrophobic drug, it is polar and water-soluble and thus systemically applicable. Thus, we turned to an *in vivo* treatment of a human DLBCL-xenograft model in mice by intra-peritoneal (i.p.) application of the drug conjugates using two different dosages of the conjugates, $4 \, \text{mg kg}^{-1}$ and $8 \, \text{mg kg}^{-1}$, calculated for the antibody moiety, which implicates the targeted delivery of only 15 to 30 nanomol of ibrutinib-Cy3.5 per single dose, twice a week.

Even at these low doses, αCD20-mAB-P/P-ibrutinib-Cy3.5 significantly reduced lymphoma growth to below 20 % of those of the controls in *in vivo* NOD-Scid gamma (NSG) mouse xenografts of HBL1 lymphomas (see Figure 6). Because the majority of the control animals had to be sacrificed due to excessive tumor growth, the tumor growth
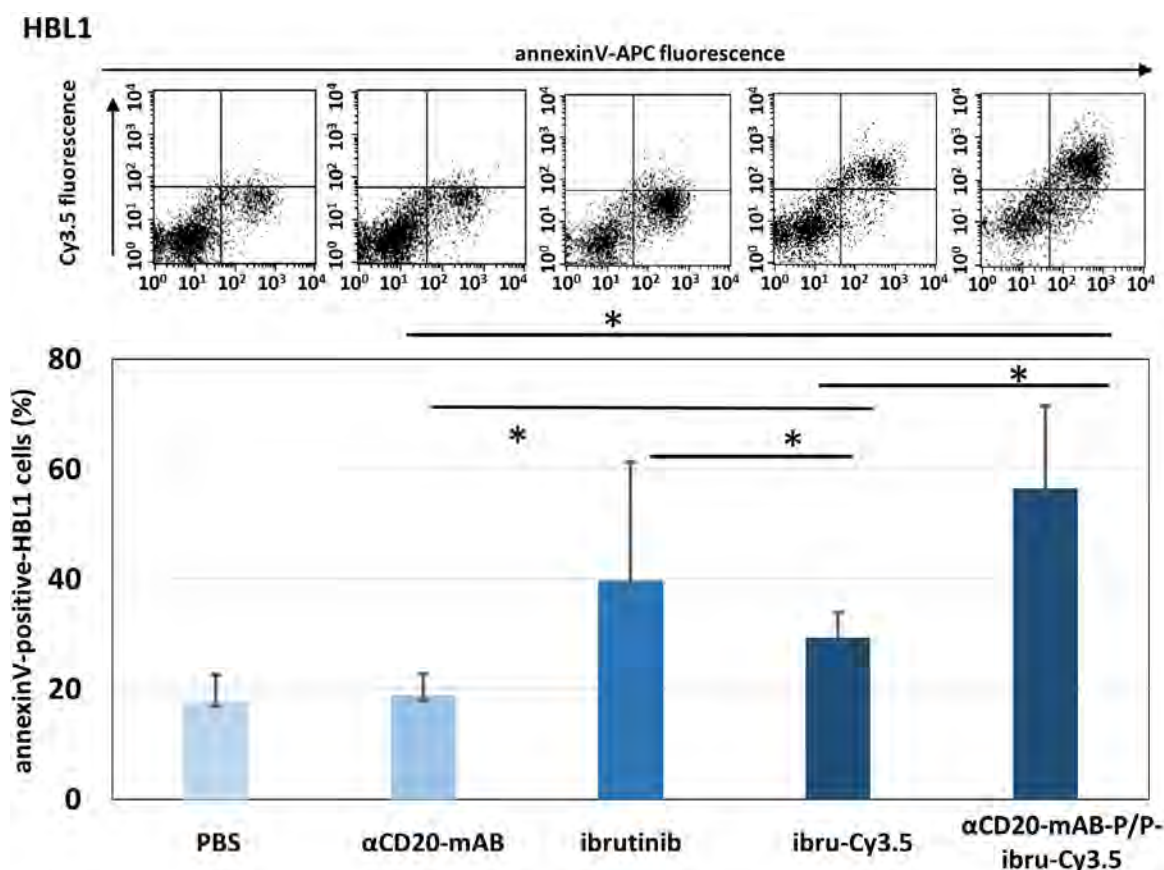
**Figure 5.** Induction of apoptosis of BTK targeting by αCD20-mAB-P/P complexed ibrutinib-Cy3.5 treatment in the DLBCL cell line HBL1. HBL1 cells were treated by the respective conjugates shown for 72 hrs and subjected to AnnexinV-staining. Apoptotic cells were detected by AnnexinV-expression (upper panel, X-Axis) by flow cytometry, while increased internalized ibrutinib-Cy3.5 fluorescence is seen by fluorescence in Y-axis (upper panel) especially in the αCD20-mAB-P/P complexed ibrutinib-Cy3.5 treated cells. Values from upper right and lower right gates were counted. Lower panel: AnnexinV-positive cells in three independent experiments were summarized. $P < 0.05$, 2-sided T-test. α, anti.

curve had to be discontinued and then was converted to a survival curve (see Kaplan-Meyer plot in Figure 6B). While the control groups, that is, the ibrutinib-Cy3.5 monotherapy, the carrier antibody as single therapy, and PBS had to be terminated on day 9 and 16, respectively, the group that received the unmodified ibrutinib (15 or 30 nmol per single dose, intra-peritoneal application) survived until day 22 (Figure 6B). In contrast, the i.p. treatment with 4 mg kg$^{-1}$ αCD20-mAB-P/P-ibrutinib-Cy3.5 led to survival up to 36 days after treatment start (Figure 6B). In a second experiment (Figure 6C,D), we used the same xenograft model of HBL1 cells in NSG mice to test the application of 8 mg kg$^{-1}$ αCD20-mAB-P/P-ibrutinib-Cy3.5 along with its respective controls. This time, we introduced a special control group into the survey, which was the combination of the un-modified αCD20-mAB combined with the Cy3.5-conjugated ibrutinib derivate. This combination was ineffective to suppress colony growth (Figure 4) and was not able to form electrostatic aggregates (not shown). In this *in vivo* experiment, the combination of 8 mg kg$^{-1}$ αCD20-mAB plus ibrutinib-Cy3.5 equally did not slow down tumor growth (violet curves in Figure 6C, lower panel) and did not show a positive effect on survival (Figure 6D).

In contrast, the 8 mg kg$^{-1}$ αCD20-mAB-P/P-ibrutinib-Cy3.5 combination effectively slowed down tumor growth to less than 20% (Figure 6C, lower panel) and prolonged survival to more than 40 days compared to 10/20 days (Figure 6D), when the experiment had to be terminated for reasons of animal welfare.

After sacrificing the mice, organs were prepared and subjected to an *in vivo* biodistribution study by *ex vivo* analysis of Cy3.5-dependent fluorescence signals. Here, in contrast to ibrutinib-Cy3.5-monotherapy treated mice (Figure 7E–G), αCD20-mAB-P/P-ibrutinib-Cy3.5 treated mice showed marked enrichment of Cy3.5-dependent fluorescence signals within the tumor tissue (Figure 7H–J), but no sequestration of Cy3.5-fluorescence signals to non-tumor tissues (Figure 7I), all seen by *ex vivo* imaging of mouse organs.

In patients, free ibrutinib (Imbruvica$^R$) is given orally at 560 mg per day, which would account for a dosage of 7.5 mg per kg for an average 75 kg adult. With due caution since parameters used in different experimental models cannot be directly compared, in previous preclinical mouse experiments, ibrutinib was applied orally in a dose from 6 mg kg$^{-1}$,[20] 12 mg kg$^{-1}$[21] or up to 50 mg kg$^{-1}$[22] showing weak anti-lymphoma effects as a single drug in human xenograft and
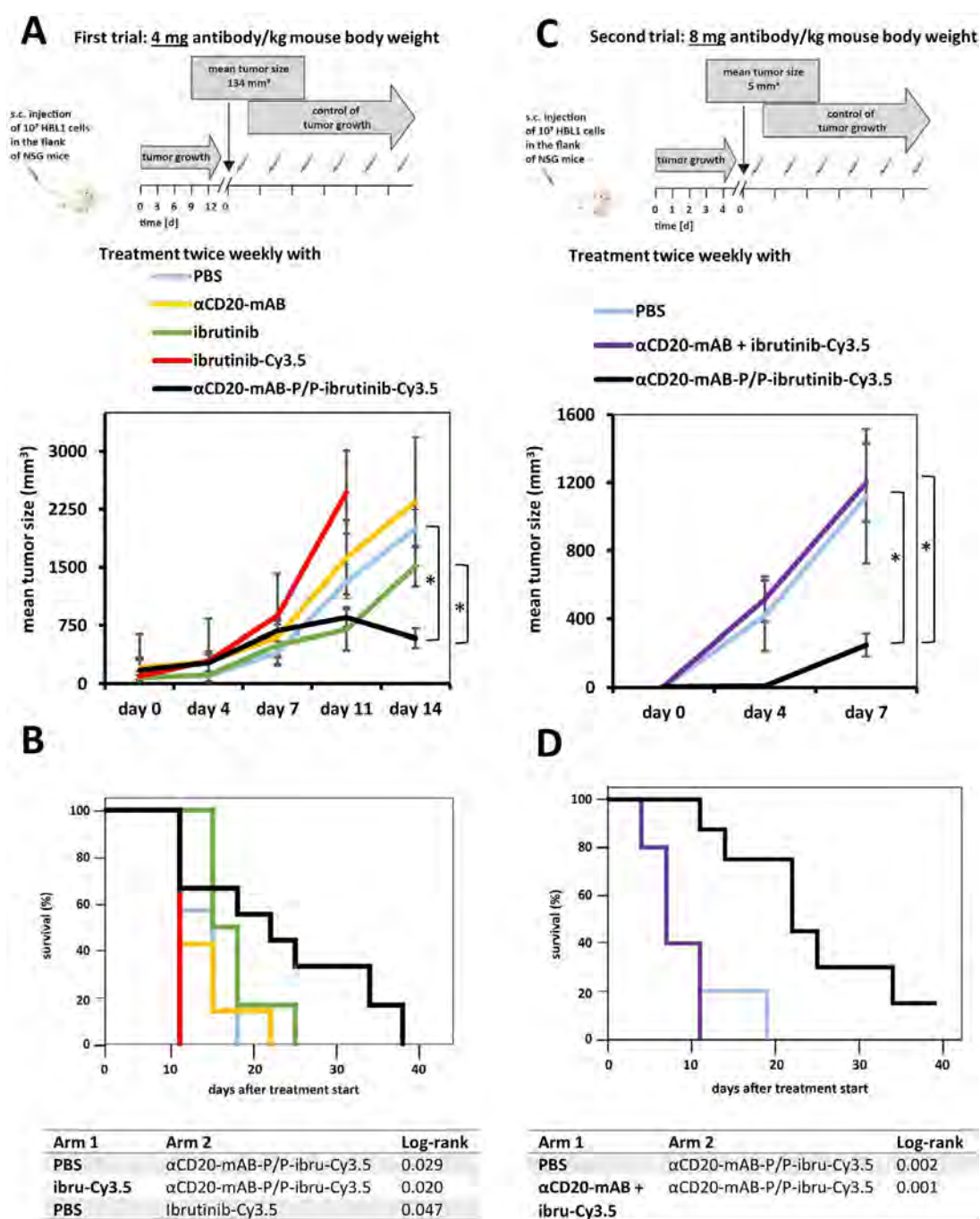
**Figure 6.** *In vivo* application of αCD20-mAB-P/P-ibrutinib-Cy3.5 to HBL1 mouse xenografts reduces tumor growth and prolongs survival. **A:** HBL1 cells were subcutaneously transplanted to NOD-Scid gamma (NSG) immunodeficient mice, tumors developed to a palpable mean size of 134 +/- 80 mm³, then mice were randomized to treatment groups and treated with PBS control, 4 mg kg⁻¹ αCD20-mAB, non-modified free ibrutinib (15 nmol (trial A) or 30 nmol (trial B) per single application, i.p.), ibrutinib-Cy3.5 (15 nmol (trial A) or 30 nmol (trial B) per single application, i.p.) and 4 mg kg⁻¹ of αCD20-mAB-P/P-ibrutinib-Cy3.5 conjugate twice a week. Below: Tumors of mice treated with PBS and all the respective monotherapy controls excessively continued to grow to day 14, when the most animals had to be sacrificed because of legal regulations, whereas only the 4 mg kg⁻¹ αCD20-mAB-P/P-ibrutinib-Cy3.5 group decreased in median tumor volume. **B:** After the termination of the tumor growth curve survey in A, the experiment was continued as a survival curve (Kaplan-Meyer plot). While the ibrutinib-Cy3.5 and the PBS group had to be terminated on days 9 and 16, respectively, the un-modified ibrutinib-treated group (ibrutinib) survived to day 22. Conversely, the αCD20-mAB-P/P-ibrutinib-Cy3.5 treated mice showed a much more decreased tumor growth and consequently the mice survived until day 36. **C:** Here, we repeated the xenograft model treatment, but starting at day 4 after transplantation at a mean tumor size of 5 mm³ with the administration of the elevated dose of 8 mg kg⁻¹ of the αCD20-mAB-P/P-ibrutinib-Cy3.5, along with the control of un-modified αCD20-mAB plus ibrutinib-Cy3.5 exposing no electrostatic assembly (violet) of the drug. The latter group was ineffective to slow down tumor growth in contrast to the 8 mg kg⁻¹ αCD20-mAB-P/P-ibrutinib-Cy3.5 which reduced tumor growth to below 20%. **D:** Likewise, the experiment was continued as a survival curve, where the 8 mg kg⁻¹ αCD20-mAB-P/P-ibrutinib-Cy3.5 (black line) survived up to 40 days post treatment in contrast to controls (between 10 and 20 days). α, anti.

*Angew. Chem. Int. Ed.* **2022**, *61*, e202109769 (8 of 11)

© 2021 The Authors. Angewandte Chemie International Edition published by Wiley-VCH GmbH
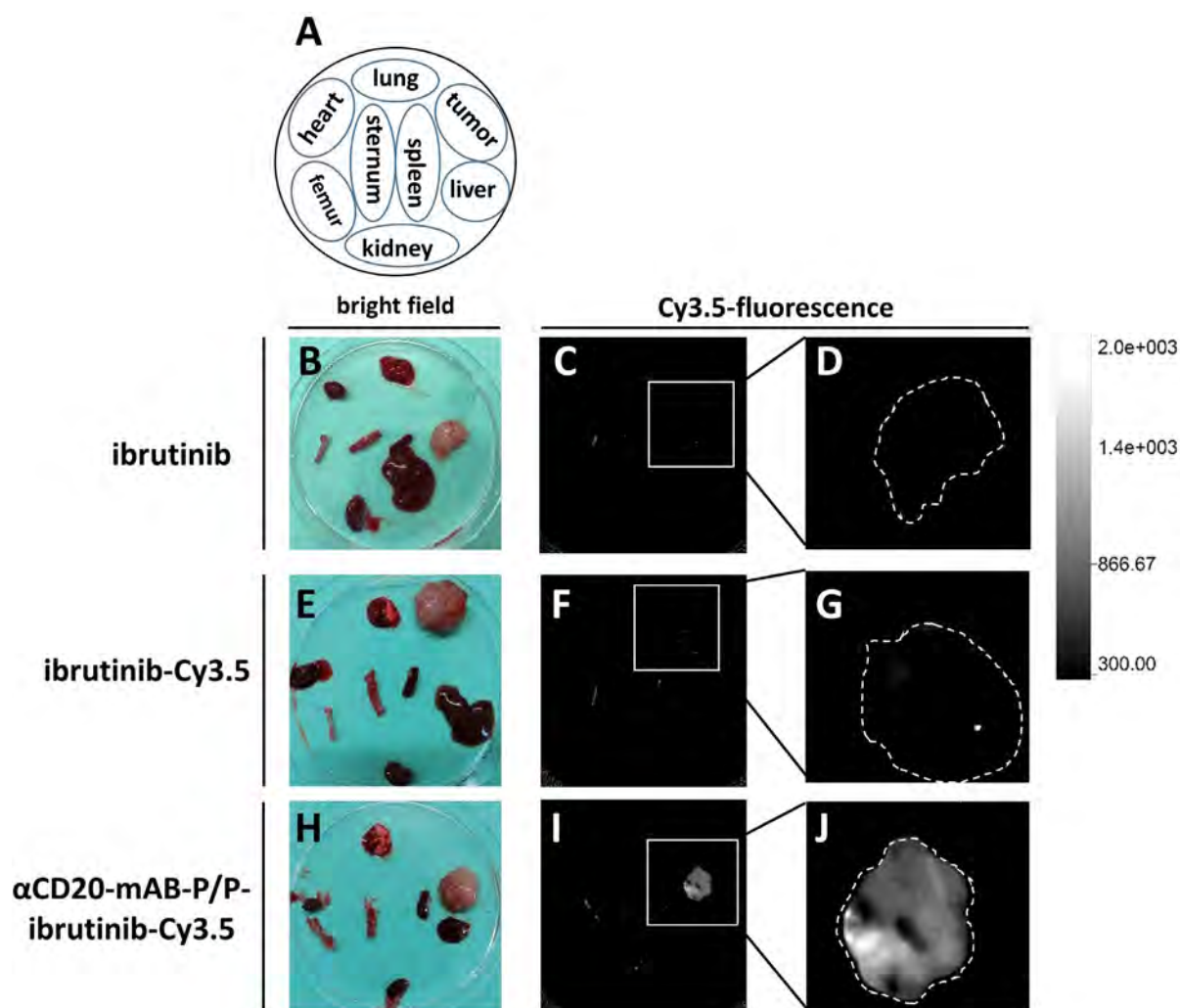
**Figure 7.** Biodistribution and tumor enrichment of αCD20-mAB-P/P-ibrutinib-Cy3.5 nanocarrier. **A:** Schematic overview of organs and tumors prepared from the treatment groups shown in B-J. Organs are always arranged in the same orientation (as depicted in the Scheme in A) in bright field (B, E, H) and red (Cy3.5) fluorescence (C–D, F–G, I–J). **B–D:** Ibrutinib-treated organs. **E–G:** ibrutinib-Cy3.5 treated organs. **H–J:** αCD20-mAB-P/P-ibrutinib-Cy3.5 treated organs. Significant Cy3.5-bound fluorescence signals were only detected in the tumor site, the fluorescence signal observed in the femur in all groups is caused by autofluorescence (I). D, G, J: Detailed analysis of tumors from C, F, I, respectively. The outer rim of the tumors were outlined (broken white line). Consistent fluorescence was only seen in tumors of the αCD20-mAB-P/P-ibrutinib-Cy3.5 treatment group. Scale in the upper panel represents arbitrary units of fluorescence. α, anti.

murine lymphoma models. Taking this dosage into account, ibrutinib was therefore applied in 410 to 3400 nanomol per single dose, respectively. In contrast, we applied only between 15 and 30 nanomol of ibrutinib-Cy3.5, targeted by 0.75–1.5 nanomol of nanocarrier as a systemic and parenteral single dose only twice a week, which is up to two orders of magnitude less than the untargeted ibrutinib applied orally. This results in much stronger anti-lymphoma effects as seen in the preclinical models cited before. After the treatments, clinical parameters for liver toxicity were recorded (Support. Figure 9), exhibiting significantly lower GOT and GPT values in αCD20-mAB-P/P-ibrutinib-Cy3.5 treated mice versus those treated with the untargeted ibrutinib, which points towards an effective concentration event of the drug in the tumor cells, but not other cells. Our new targeting and carrier system thereby confers transport of a novel anionic form of the BTK-inhibitor ibrutinib (ibrutinib-Cy3.5) into CD20-

positive lymphoma cells *in vitro* and *in vivo*. The conjugate has the potential to spare the CD20-negative cells *in vivo* and therefore to concentrate the ibrutinib derivate specifically in CD20-expressing lymphoma cells and tumors. There it is internalized by CD20-receptor mediated endocytosis as known for type I αCD20-mABs[23] and subsequently most likely undergoes endosomal maturation via protonation.[24] Release first from the protamine and second from the endosome during this process by protamine-dependend endosomal destabilization events was also observed by others.[25] However, this will be a subject of further investigations.

*In vitro*, this novel ibrutinib derivate thereby showed the same intracellular effects than unmodified ibrutinib, which means that the derivatization to a poly-anionic structure imposes no disadvantage in terms of reactivity towards the target cysteine in the BTK ATP binding pocket. Strikingly, *in*

*vivo*, tumor growth was significantly inhibited when αCD20-mAB-P/P-ibrutinib-Cy3.5 was applied, while the same concentrations of unconjugated αCD20-mAB combined with free ibrutinib-Cy3.5 were not successful to slow tumor growth, which means that *in vivo*, it shows a major improvement of biotargeting of the ibrutinib compound towards tumor tissues. Of note, only tumors treated with the targeted conjugate αCD20-mAB-P/P-ibrutinib-Cy3.5 showed distinct detectable Cy3.5-fluorescence in *ex vivo* biodistribution studies, indicating that normal mouse organs were not affected and that the targeted nanocarrier system concentrated ibrutinib-Cy3.5 specifically within the tumor.

We found that the therapeutic effect of ibrutinib-Cy3.5 is imperatively dependent on its electrostatic assembly and delivery by assembly into the carrier antibody αCD20-mAB-P/P construct, which guides the kinase inhibitor to the intended target cells, concentrates it in the cells and amplifies its biological function at two orders of magnitude, according to the much lower dosages necessary. This observation strongly supports the new and unexpected macromolecular nanostructure as being necessary and sufficient for the *in vitro* and *in vivo* pharmacodynamic efficacy of our carrier system. Also, we found that the electrostatic complex between the ibrutinib-Cy3.5 polyanion and the antibody-protamine conjugate requires unconjugated protamine as an "electrostatic glue" between both components, leading to stable nanoparticles of a reproducible size distribution. For instance, when we purified the conjugate mixture from excess protamine (Figure 4B and Support. Figure 7B), the formation of the nanocarrier was not observed and the resulting component mixture was not effective in colony assays.

These findings are in contrast to those published for the unconjugated ibrutinib drug, which is given orally, which is known to affect and target cells independent of their origin, and which shows a 90% irreversible absorption of given dosage by plasma proteins and more than 80% rapid clearance and excretion mostly in faeces.[26]

Furthermore, it was observed that ibrutinib also binds to other kinases containing the similar reserved cysteine residue such as the epidermal growth factor receptor (EGFR), human EGFR 2 (HER2/neu), human EGFR 4 (HER4/ErbB4), interleukin-2-inducible T-cell kinase (ITK), and Janus kinase 3. As they also have a cysteine residue at analogous position[27] inside the ATP-binding pocket, an ibrutinib binding to those will lead to considerable loss of available drug. As one example, ibrutinib displays significant BTK-independent effects on the T-cell lineage, which is in agreement with previous studies reporting that T-cell activation is blocked by irreversible binding of ibrutinib to ITK.[13,28] Our antibody-drug nanocarrier wraps anionic ibrutinib-Cy3.5 and transports it preferentially into CD20-positive cells. Since CD20-positive T-cells are extremely rare,[29] one can assume that our transport system spares T-cells.

## Conclusion

To our knowledge, this is the first time that an anionic drug-derivative assembles by electrostatic interactions with a cationic carrier system consisting of cationic protamine, which in turn was decorated with a cell target-specific antibody.

Our electrostatic assembly of drug-cargo to carrier-antibody imposes a number of major improvements: First, the multiplication of the cargo-to-carrier ratio, second the concentration of the drug at the desired place of action and last the selective process of molecular intervention. Moreover, our nanocarrier offers the possibility of being used as a platform technology with a broad target cell spectrum: a change of the targeting antibody from αCD20-mAB-protamine to αCD33-mAB-protamine would change the range of targeted cells from the B-cell lineage to myeloid cells in myeloid leukemia[30,31] and the change to αEGFR-mAB-protamine to solid tumor cells in lung cancer.[32,33] On the effector side, an exchange from ibrutinib-polyanion to a small molecular inhibitor with other pharmacodynamic properties could change the therapeutic warhead towards other pharmacological targets and modes of action.

## Conflict of Interest

AF, NB, LW, GL, and WEB have filed 2 patent applications on nanocarrier technology. The other authors declare no conflict of interest.

[1] R. L. Schilsky, S. Nass, M. M. Le Beau, E. J. Benz, *N. Engl. J. Med.* **2020**, *383*, 897.

[2] N. Joubert, A. Beck, C. Dumontet, C. Denevault-Sabourin, *Pharmaceuticals* **2020**, *13,* 245.

[3] P. Khongorzul, C. J. Ling, F. U. Khan, A. U. Ihsan, J. Zhang, *Mol. Cancer Res.* **2020**, *18*, 3.

[4] K. Tsuchikama, Z. An, *Protein Cell* **2018**, *9*, 33.

[5] V. H. van der Velden, J. G. te Marvelde, P. G. Hoogeveen, I. D. Bernstein, A. B. Houtsmuller, M. S. Berger, J. J. van Dongen, *Blood* **2001**, *97*, 3197.

[6] R. A. de Claro, K. M. McGinn, N. Verdun, S.-L. Lee, H.-J. Chiu, H. Saber, M. E. Brower, C. J. G. Chang, E. Pfuma, B. Habte-mariam, et al., *Clin. Cancer Res.* **2015**, *21*, 3586.

[7] V. Kaur, A. Swami, *Ann. Hematol.* **2017**, *96*, 1175.

[8] a) N. A. Amin, S. Balasubramanian, K. Saiya-Cork, K. Shedden, N. Hu, S. N. Malek, *Clin. Cancer Res.* **2017**, *23*, 1049; b) G. Del Poeta, M. Postorino, F. Pozzo, M. I. Del Principe, E. Santinelli, R. Bomben, A. Biagi, F. Buccisano, F. M. Rossi, A. Venditti, et al., *Blood* **2018**, *132*, 4397.

[9] G. Lenz, *J. Clin. Oncol.* **2017**, *35*, 1451.

[10] a) S. Bäumer, N. Bäumer, N. Appel, L. Terheyden, J. Fremerey, S. Schelhaas, E. Wardelmann, F. Buchholz, W. E. Berdel, C. Müller-Tidow, *Clin. Cancer Res.* **2015**, *21*, 1383–94; b) N. Bäumer, J. Rehkämper, N. Appel, L. Terheyden, W. Hartmann, E. Wardelmann, F. Buchholz, C. Müller-Tidow, W. E. Berdel, S. Bäumer, *PLoS One* **2018**, *13*, e0200163; c) N. Bäumer, N. Appel, L. Terheyden, F. Buchholz, C. Rossig, C. Müller-Tidow, W. E. Berdel, S. Bäumer, *Nat. Protoc.* **2016**, *11*, 22.

[11] a) D. Hoelzer, *Curr. Opin. Oncol.* **2013**, *25*, 701; b) T. L. Naylor, H. Tang, B. A. Ratsch, A. Enns, A. Loo, L. Chen, P. Lenz, N. J. Waters, W. Schuler, B. Dorken, et al., *Cancer Res.* **2011**, *71*, 2643; c) H. Nogai, B. Dorken, G. Lenz, *J. Clin. Oncol.* **2011**, *29*, 1803.

[12] J. Chen, T. Kinoshita, J. Sukbuntherng, B. Y. Chang, L. Elias, *Mol. Cancer Ther.* **2016**, *15*, 2835.

[13] J. A. Dubovsky, K. A. Beckwith, G. Natarajan, J. A. Woyach, S. Jaglowski, Y. Zhong, J. D. Hessler, T.-M. Liu, B. Y. Chang, K. M. Larkin, et al., *Blood* **2013**, *122*, 2539.

[14] J. C. Byrd, R. R. Furman, S. E. Coutre, I. W. Flinn, J. A. Burger, K. A. Blum, B. Grant, J. P. Sharman, M. Coleman, W. G. Wierda, et al., *N. Engl. J. Med.* **2013**, *369*, 32.

[15] a) C. Gisselbrecht, B. Glass, N. Mounier, D. Singh Gill, D. C. Linch, M. Trneny, A. Bosly, N. Ketterer, O. Shpilberg, H. Hagberg, et al., *J. Clin. Oncol.* **2010**, *28*, 4184; b) R. R. Furman, J. P. Sharman, S. E. Coutre, B. D. Cheson, J. M. Pagel, P. Hillmen, J. C. Barrientos, A. D. Zelenetz, T. J. Kipps, I. Flinn, et al., *N. Engl. J. Med.* **2014**, *370*, 997.

[16] W. H. Wilson, R. M. Young, R. Schmitz, Y. Yang, S. Pittaluga, G. Wright, C. J. Lih, P. M. Williams, A. L. Shaffer, J. Gerecitano, et al., *Nat. Med.* **2015**, *21*, 922.

[17] a) E. Kim, K. S. Yang, R. H. Kohler, J. M. Dubach, H. Mikula, R. Weissleder, *Bioconjugate Chem.* **2015**, *26*, 1513; b) A. Turetsky, E. Kim, R. H. Kohler, M. A. Miller, R. Weissleder, *Sci. Rep.* **2014**, *4*, 4782.

[18] N. Liu, S. Hoogendoorn, B. van de Kar, A. Kaptein, T. Barf, C. Driessen, D. V. Filippov, G. A. van der Marel, M. van der Stelt, H. S. Overkleeft, *Org. Biomol. Chem.* **2015**, *13*, 5147.

[19] a) M. Abdul Ghafoor Raja, H. Katas, T. Jing Wen, *PLoS One* **2015**, *10*, e0128963; b) Y. Xia, M. Zhao, Y. Chen, L. Hua, T. Xu, C. Wang, Y. Li, B. Zhu, *RSC Adv.* **2018**, *8*, 25932.

[20] I. Sagiv-Barfi, H. E. Kohrt, L. Burckhardt, D. K. Czerwinski, R. Levy, *Blood* **2015**, *125*, 2079.

[21] H.-P. Kuo, S. A. Ezell, K. J. Schweighofer, L. W. K. Cheung, S. Hsieh, M. Apatira, M. Sirisawad, K. Eckert, S. J. Hsu, C.-T. Chen, et al., *Mol. Cancer. Ther.* **2017**, *16*, 1246.

[22] I. Muqbil, M. Chaker, A. Aboukameel, R. M. Mohammad, A. S. Azmi, R. Ramchandren, *Heliyon* **2019**, *5*, e02290.

[23] G. Pavlasova, M. Mraz, *Haematologica* **2020**, *105*, 1494.

[24] N. Bäumer, W. E. Berdel, S. Bäumer, *Mol. Pharm.* **2017**, *14*, 1339.

[25] a) N. T. Jarzebska, M. Mellett, J. Frei, T. M. Kündig, S. Pascolo, *Pharmaceutics* **2021**, *13*, 877; b) R. S. Shukla, A. Jain, Z. Zhao, K. Cheng, *Nanomedicine* **2016**, *12*, 1323.

[26] E. Scheers, L. Leclercq, J. de Jong, N. Bode, M. Bockx, A. Laenen, F. Cuyckens, D. Skee, J. Murphy, J. Sukbuntherng, et al., *Drug Metabolism Disposition* **2015**, *43*, 289.

[27] Z. Pan, H. Scheerens, S.-J. Li, B. E. Schultz, P. A. Sprengeler, L. C. Burrill, R. V. Mendonca, M. D. Sweeney, K. C. K. Scott, P. G. Grothaus, et al., *ChemMedChem* **2007**, *2*, 58.

[28] H. Y. Estupiñán, T. Bouderlique, C. He, A. Berglöf, D. Gupta, O. Saher, M. Á. Daza Cruz, L. Peña-Perez, L. Yu, R. Zain, et al., *Blood Adv.* **2020**, *4*, 2439.

[29] S. Gingele, T. Skripuletz, R. Jacobs, *Neural Regener. Res.* **2020**, *15*, 663.

[30] S. A. Rushworth, M. Y. Murray, L. Zaitseva, K. M. Bowles, D. J. MacEwan, *Blood* **2014**, *123*, 1229.

[31] a) M. E. Davis, J. E. Zuckerman, C. H. Choi, D. Seligson, A. Tolcher, C. A. Alabi, Y. Yen, J. D. Heidel, A. Ribas, *Nature* **2010**, *464*, 1067; b) C. A. Eide, S. E. Kurtz, A. Kaempf, N. Long, A. Agarwal, C. E. Tognon, M. Mori, B. J. Druker, B. H. Chang, A. V. Danilov, et al., *Leukemia* **2020**, *34*, 2342.

[32] J. Gao, Y. Yu, Y. Zhang, J. Song, H. Chen, W. Li, W. Qian, L. Deng, G. Kou, J. Chen, et al., *Biomaterials* **2012**, *33*, 270.

[33] D. Hong, D. Rasco, M. Veeder, J. J. Luke, J. Chandler, A. Balmanoukian, T. J. George, P. Munster, J. D. Berlin, M. Gutierrez, et al., *Oncology* **2019**, *97*, 102.

# Tumor-Cell-Specific Targeting of Ibrutinib: Introducing Electrostatic Antibody-Inhibitor Conjugates (AiCs)

*Andreas Faust+, Nicole Bäumer+, Alina Schlütermann, Manuel Becht, Lilo Greune, Christiane Geyer, Christian Rüter, Renato Margeta, Lisa Wittmann, Petra Dersch, Georg Lenz, Wolfgang E. Berdel, and Sebastian Bäumer\**

anie_202109769_sm_miscellaneous_information.pdf

# Supporting Information

**Content**

## 1. Synthesis of Cy3.5-ibrutinib

### 1.1. General information

All solvents and reagents were used as received from commercial suppliers unless otherwise stated. Reaction progress was monitored by TLC performed on aluminium plates coated with silica gel 60 $F_{254}$ from Merck (Darmstadt, Germany). Chromatograms were visualized by fluorescence quenching with UV light at $\lambda=254$ nm and by staining with iodine vapour or ninhydrin staining solution. Column chromatography was performed using silica gel 60 (230-400 mesh, Merck) or prepacked columns Büchi FlashPure silica 40 μm irregular, using a Grace Reveleris X2 flash purification system. Some reactions were performed in microwave reactor CEM Discover. For solid separation was used Eppendorf Centrifuge 5804R. Melting points were measured on Mettler Toledo MP70 Melting Point System. NMR-spectra were obtained at the Organisch-Chemisches Institut Münster (WWU), using an Agilent DD2 500/ Agilent DD2 600 or a Bruker Avance II 400. All measurements were performed at room temperature unless mentioned otherwise. The $^1$H-NMR and $^{13}$C-NMR chemical shifts (δ) of the signals are given in parts per million and are referenced to the residual proton signal in the deuterated solvent. The signal multiplicities are abbreviated as follows: s, singlet; bs, broad singlet; d, doublet; t, triplet; q, quartet; m, multiplet.

Exact mass (EM) determination by mass spectrometry (MS) was carried out at the Organisch-Chemisches Institut Münster (WWU) using a LTQ Orbitap LTQ XL (Thermo-Fisher Scientific, Bremen, Germany) with electron spray ionisation (ESI).

HPLC chromatograms were made on Knauer (Berlin, Germany) HPLC system equipped with the pump P2.1L and diode array detector DAD6.1L.

## 1.2 Synthesis

### 1.2.1 3-(4-phenoxyphenyl)-1H-pyrazolo[3,4-d]pyrimidine-4-amine (2) [1]
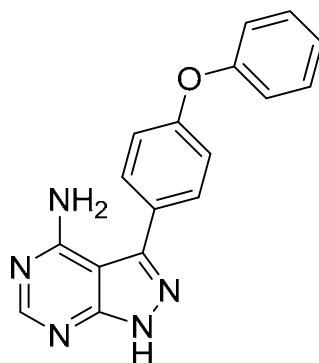


Iodide **1** (1000 mg, 3.85 mmol, 1.0 eq.), 4-phenoxyphenylboronic acid (823 mg, 3.85 mmol, 1.0 eq.) and tetrakis-(triphenylphosphine)palladium (444 mg, 0.38 mmol, 0.1 eq.) were suspended in dioxane (10 mL) and potassium hydroxide (431 mg, 7.69 mmol, 2.0 eq.) dissolved in water (2 mL) was added. The reaction mixture was irradiated 10 minutes on 180°C in microwave reactor. The resulting reaction mixture was diluted with EtOAc (80 mL) and water (20 mL) and layers were separated. The aqueous layer was additionally extracted with 3 x 20 mL EtOAc. Organic layers were combined, washed with brine and dried over anhydrous $MgSO_4$. The solvent was removed under reduced pressure and residue was triturated four times with DCM and dried on high vacuum to give 668 mg of product **2** (2.20 mmol, 58%) as a white powder.

$^1$H NMR (400MHz, DMSO-$d_6$): δ = 13.58 (s, 1H, NH), 8.22 (s, 1H, CH), 7.67 (d, 2H, $J$=8.7Hz, PhH), 7.45-7.40 (m, 2H, PhH), 7.20-7.10 (m, 5H, PhH).

$^{13}$C NMR (100MHz, DMSO-$d_6$): δ = 158.1, 157.0, 156.3, 156.1, 155.8, 143.9, 130.1, 130.0, 128.5, 123.8, 119.0, 118.9, 96.9.

TLC (silica, 10% MeOH / CHCl$_3$, det.: UV$_{254nm}$ & J$_2$): R$_f$ = 0.37

HRMS (ESI+): exact mass calculated for [M+H]$^+$ ($C_{17}H_{14}N_5O$) required *m/z* 304.1193; found *m/z* 304.1198.

---

[1] slightly modified from A. Turetsky, E. Kim, R. H. Kohler, M. A. Miller, R. Weissleder, *Sci. Rep.* **2014**, *4*, 4782.

### 1.2.2 (*S*)-3-Mesyl-N-Boc-piperidine (3) [2]
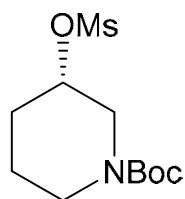


(*S*)-3-hydroxy-*N*-Boc-piperidine (13.0 g, 65 mmol, 1 eq.) was dissolved in DCM (100 mL) and triethylamine (20 mL, 14.4 g, 143 mmol, 2.2 eq.) was added. With cooling on -5°C methanesulfonyl chloride (6.5 mL, 9.6 g, 84 mmol, 1.3 eq.) was added dropwise and after that the reaction mixture was stirred on room temperature overnight. The reaction mixture was diluted with water (100 mL) and layers were separated. Organic layer was washed with 0.1M HCl until aqueous layer be in the range pH=3-4. Combined aqueous layers were additionally extracted with 2 x 100 mL DCM. Combined organic layers were washed with brine and dried over anhydrous $MgSO_4$. The solvent was removed under reduced pressure to give 13.9 g of product **3** (49.80 mmol, 77%) as a white solid.

$^1$H NMR (400MHz, $CDCl_3$): δ = 4.72-4.67 (m, 1H, CH), 3.66-3.54 (m, 2H, CH), 3.46-3.38 (m, 1H, CH), 3.33-3.25 (m, 1H, CH), 3.02 (s, 3H, CH), 1.96-1.74 (m, 3H, CH), 1.55-1.43 (m, 1H, CH), 1.43 (s, 9H, CH).

$^{13}$C NMR (100MHz, $CDCl_3$): δ = 154.8, 80.2, 75.5, 47.5, 43.1, 38.8, 30.5, 28.4, 21.7.

TLC (silica, cyclohexane / EtOAc 1:2 v/v, det.: $UV_{254nm}$ & $J_2$): $R_f$ = 0.60

HRMS (ESI+): exact mass calculated for $[M+Na]^+$ ($C_{11}H_{21}NO_5SNa$) required *m/z* 302.1038; found *m/z* 302.1048.

---

[2] according to WO2017/137446 (PCT/EP2017/052773).

### 1.2.3  (*R*)-*tert*-butyl    3-(4-amino-3-(4-phenoxyphenyl)-1H-pyrazolo[3,4-d]pyrimi-dine-1-yl)-piperidine-1-carboxylate (4) [3]
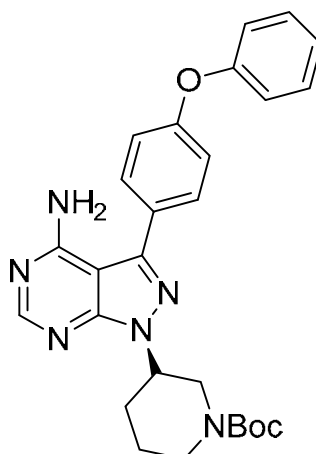


Amine **2** (1 g, 3.30 mmol, 1.0 eq.) and mesylate **3** (1.84 g, 6.60 mmol, 2.0 eq.) were dissolved in DMF (40 mL) and reaction mixture was stirred on 80°C overnight and then cooled to the room temperature and poured into water (1 L). Obtained emulsion was saturated with crude NaCl and extracted with 3 x 200 mL EtOAc. Combined organic layers were washed with brine and dried over anhydrous $MgSO_4$. The solvent was removed under reduced pressure and residue was triturated with 3 x 20 mL pentane. Obtained crude product was purified by flash chromatography on 80g silica column with 0->60% EtOAc / cyclohexane as eluent. Fraction, eluted with EtOAc / cyclohexane 1:1, was evaporated to give 730 mg of product **4** (1.50 mmol, 46%) as a white foam.

$^{1}$H NMR (500MHz, $CDCl_3$): δ = 8.28 (s, 1H, CH), 7.58 (d, 2H, *J*=8.6Hz, PhH), 7.32-7.29 (m, 2H, PhH), 7.09-7.07 (m, 3H, PhH), 7.01-6.99 (m, 2H, PhH), 5.80 (bs, 2H, NH), 4.79-4.73 (m, 1H, CH), 4.06-4.02 (m, 1H, CH), 3.41-3.38 (m, 1H, CH), 2.78 (td, 1H, *J*=12.8Hz, 2.9Hz, CH), 2.24-2.08 (m, 2H, CH), 1.84-1.81 (m, 1H, CH), 1.67-1.56 (m, 1H, CH), 1.37 (s, 9H, CH).

$^{13}$C NMR (125MHz, $CDCl_3$): δ = 158.5, 157.9, 156.4, 155.6, 154.7, 154.2, 143.8, 130.0, 130.0, 127.9, 124.0, 119.5, 119.1, 98.6, 79.9, 53.0, 47.5, 43.5, 30.2, 28.4.

TLC (silica, cyclohexane / EtOAc 1:1 v/v, det.: $UV_{254nm}$ & ninhydrin sol.): $R_f$ = 0.32 (blue fluorescence at $UV_{254nm}$)

HRMS (ESI+): exact mass calculated for $[M+H]^+$ ($C_{27}H_{31}N_6O_3$) required *m/z* 487.2458; found *m/z* 487.2461.

[3] slightly modified from A. Turetsky, E. Kim, R. H. Kohler, M. A. Miller, R. Weissleder, *Sci. Rep.* **2014**, *4*, 4782.

### 1.2.4. *N*-Boc-2-aminoacetaldehyde (5) [4]

$$\text{O} \quad \text{NHBoc}$$
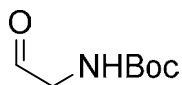
Into suspension of *tert*-butyl N-(2,3-dihydroxypropyl)carbamate (2.00 g, 10.47 mmol, 1 eq.) in water (17.5 mL), NaIO$_4$ (2.69g, 12.564 mmol, 1.2 eq.) was added and reaction mixture was stirred on room temperature, protected from the light. After 1 hour reaction mixture was filtered and filtrate was extracted with 4 x 50 mL DCM. Combined organic layers were washed with brine and dried over anhydrous MgSO$_4$. The solvent was removed under reduced pressure to give 1.40 g of product **5** (8.80 mmol, 84%) as a colorless oil.

$^1$H NMR (400MHz, CDCl$_3$): δ = 9.58 (s, 1H, CHO), 5.20 (bs, 1H, NH), 4.00 (d, 2H, $J_{H,H}$=5.1Hz, CH), 1.39 (s, 9H, CH).

TLC (silica, cyclohexane / EtOAc 1:1 v/v, det.: UV$_{254nm}$ & ninhydrin): R$_f$ = 0.43

### 1.2.5. Ethyl (*E*)-4-((*tert*-butoxycarbonyl)amino)but-2-enoate (6) [4]

$$\text{BocHN} \diagup\diagdown \diagup \text{COOEt}$$
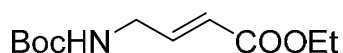
Sodium hydride (60% dispersion in mineral oil) (387 mg, 9.69 mmol, 1.1 eq.) was suspended in dry THF. With cooling on 0$^o$C, solution of triethyl phosphonoacetate (1.92 mL, 9.69 mmol, 1.1 eq.) in 5 mL dry THF was added dropwise. After 20 minutes, solution of aldehyde **5** (1.40 g, 8.81 mmol, 1 eq.) dissolved in 5 mL dry THF was added slowly, and reaction was allowed to warm to the room temperature with tracking by TLC. After about 1 hour, when all starting aldehyde was consumed, reaction mixture was evaporated. Residue was dissolved in mixture 50 mL EtOAc + 50 mL water and layers were separated. Aqueous layer was extracted with 3 x 50 mL EtOAc. Combined all organic layers were washed with brine and dried over anhydrous MgSO$_4$. The solvent was removed under reduced pressure to give 2.30 g of crude product in form of yellow oil. Purification was performed by flash chromatography on 40 g column with

---

[4] According to US2017/0152228A1

0->50% EtOAc / cyclohexane as eluent. Collected fractions were evaporated to give 707 mg of pure product **6** (3.09 mmol, 35%) as a colourless oil.

$^1$H NMR (400MHz, CDCl$_3$): δ = 6.84 (dt, 1H, $J_{H,H}$=15.7Hz, 4.9Hz, CH), 5.86 (dt, 1H $J_{H,H}$=15.7Hz, 1.9Hz, CH), 4.74 (bs, 1H, NH), 4.12 (q, 1H, $J_{H,H}$=7.1Hz, CH), 3.84 (bs, 2H, CH), 1.33 (s, 9H, CH), 1.21 (t, 3H, $J_{H,H}$=7.2Hz, CH).

$^{13}$C NMR (100MHz, CDCl$_3$): δ = 166.1, 155.6, 144.7, 121.3, 79.8, 60.4, 41.3, 28.3, 14.3.

TLC (silica, cyclohexane / EtOAc 1:1 v/v, det.: UV$_{254nm}$ & ninhydrin): R$_f$ = 0.75

HRMS (ESI+): exact mass calculated for [M+Na]$^+$ (C$_{11}$H$_{19}$NO$_4$Na) required *m/z* 252.1212; found *m/z* 252.1212.

### 1.2.6. (*E*)-4-((*tert*-butoxycarbonyl)amino)but-2-enoic acid (7) [5]
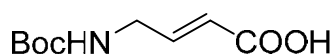


Ester **6** (670 mg, 2.93 mmol, 1 eq.) and lithium hydroxide (280 mg, 11.70 mmol, 4 eq.) were dissolved in mixture THF / water 2:1 (v/v) (30 mL) and the reaction mixture was stirred on room temperature overnight. Reaction mixture was concentrated on rotavapor to about 1/3 of volume and then extracted with 1 x 20 mL EtOAc. Aqueous layer was then acidified to pH=3-4 with saturated solution NH$_4$Cl and 5% aq.sol. citric acid, then saturated by addition of crude NaCl and extracted with 3 x 100 mL EtOAc. That last three EtOAc extracts were combined, washed with brine and dried over anhydrous MgSO$_4$. The solvent was removed under reduced pressure to give 488 mg of product **7** (2.43 mmol, 83%) as a white solid.

$^1$H NMR (400MHz, CDCl$_3$): δ = 9.92 (bs, 1H, COOH), 6.93 (dt, 1H, $J_{H,H}$=15.8Hz, 4.8Hz, CH), 5.87 (dt, 1H, $J_{H,H}$=15.6Hz, 1.9Hz, CH), 4.78 (bs, 1H, NH), 3.88 (bs, 2H, CH), 1.39 (s, 9H, CH).

$^{13}$C NMR (100MHz, CDCl$_3$): δ = 170.8, 155.7, 147.2, 120.7, 80.1, 41.4, 28.3.

TLC (silica, MeOH/CHCl$_3$ 1:9 v/v, det.: UV$_{254nm}$ & ninhydrin): R$_f$ = 0.32

HRMS (ESI+): exact mass calculated for [M+Na]$^+$ (C$_9$H$_{15}$NO$_4$Na) required *m/z* 224.0893; found *m/z* 224.0900.

---

[5] slightly modified from A. Turetsky, E. Kim, R. H. Kohler, M. A. Miller, R. Weissleder, *Sci. Rep.* **2014**, *4*, 4782.

### 1.2.7. (*R*)-3-(4-phenoxyphenyl)-1-(piperidine-3-yl)-1H-pyrazolo[3,4-d]pyrimidine-4-amine hydrochloride (8) [6]
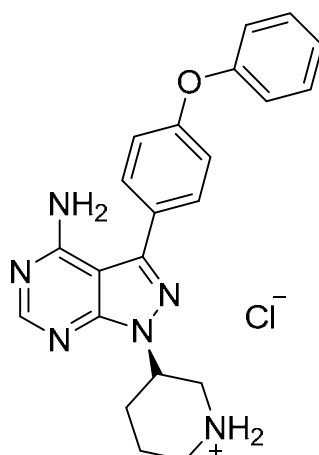


Carbamate **4** (690 mg, 1.42 mmol, 1 eq.) was dissolved in mixture EtOAc / MeOH 1:1 (v/v) (40 mL) and 4M solution of $HCl_{(g)}$ in dioxane (2.1 mL, 8.52 mmol, 6 eq.) was added. Reaction mixture was stirred on room temperature overnight. Obtained white suspension was evaporated, residual solid was triturated with pentane and ether and dried under high vacuum to give 637 mg of product **8** (1.51 mmol, 98%) as a white crystalline solid was directly used for the next step

TLC (silica, MeOH/EtOAc 1:4 v/v, det.: $UV_{254nm}$ & ninhydrin): $R_f = 0.09$

HRMS (ESI+): exact mass calculated for [M+H]+ ($C_{22}H_{23}N_6O$) required *m/z* 387.1928; found *m/z* 387.1927.

---

[6] slightly modified method from WO2017/137446 (PCT/EP2017/052773)

## 1.2.8. Ibrutinib derivative (9) [7]
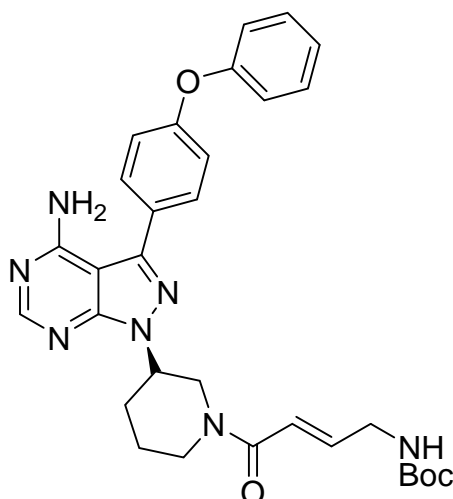


Hydrochloride **8** (300 mg, 0.71 mmol, 1 eq.) and DIPEA (740 µL, 4.27 mmol, 6 eq.) were dissolved in ACN (20 mL) and reaction mixture was stirred for 10 minutes on room temperature. PyAOP (741 mg, 1.42 mmol, 2 eq.) and acid **7** (143 mg, 0.71 mmol, 1 eq.) were dissolved separately in ACN (10 mL) and after 10 minutes that solution was added to reaction mixture with amine. Stirring was continued on room temperature with tracking by TLC. When reaction was completed, reaction mixture was evaporated, residue was dissolved in 100 mL EtOAc and washed with: 1 x 20 mL water, 1 x 20 mL 5% aq.sol. citric acid, 1 x 20 mL sat.sol. NaHCO₃, brine and dried over anhydrous MgSO₄. The solvent was removed under reduced pressure to give 896 mg of crude product **9** as brown oil. Crude product was purified by flash chromatography on 40 g silica column with 0->10% MeOH in EtOAc as eluent. Collected fractions were evaporated to give 291 mg of pure product **9** (0,511 mmol, 72%) as a white solid [8].

$^1$H NMR (300MHz, CDCl₃): δ = 8.28 (bd, 1H, NH), 7.59-7.54 (m, 2H, PhH), 7.35-7.28 (m, 2H, PhH), 7.13-6.99 (m, 5H, PhH), 6.67 (bs, 1H, CH), 6.32 (t, 1H, $J_{H.H}$=14.2Hz, CH), 5.73 (bs, 2H, NH), 4.78-4.74 (m, 2.5H, CH), 4.52-4.47 (m, 0.5H, CH), 4.12-3.63 (m, 3.5H, CH), 3.32-3.23 (m, 0.5H, CH), 3.14-3.04 (m, 0.5H, CH), 2.84-2.76 (m, 0.5H, CH), 2.23-2.10 (m, 2H, CH), 1.94-1.89 (m, 1H, CH), 1.66-1.62 (m, 1H, CH), 1.39, 1.30 (2s, 9H, CH).

---

[7] only method from *J. Am. Chem. Soc.*, (2012), **134**, 18388-18400; solvent choice from *J. Pept. Sci.*, (2009), **15**, 629-633.

[8] colorless oil obtained after evaporation was converted into white solid by precipitation from DCM/pentane

$^{13}$C NMR (75MHz, CDCl$_3$): δ = 165.5, 157.9, 155.7, 155.6, 154.2, 144.0, 130.0, 127.2, 124.1, 121.0, 119.6, 119.1, 110.0, 53.4, 50.1, 46.2, 41.8, 34.2, 28.3.

TLC (silica, MeOH/EtOAc 1:9 v/v, det.: UV$_{254nm}$ & ninhydrin): R$_f$ = 0.39 (dark blue fluorescence at UV$_{254nm}$)

HRMS (ESI+): exact mass calculated for [M+Na]$^+$ (C$_{31}$H$_{36}$N$_7$O$_4$) required *m/z* 570.2823; found *m/z* 570.2822.

### 1.2.9. Ibrutinib-Cy3.5
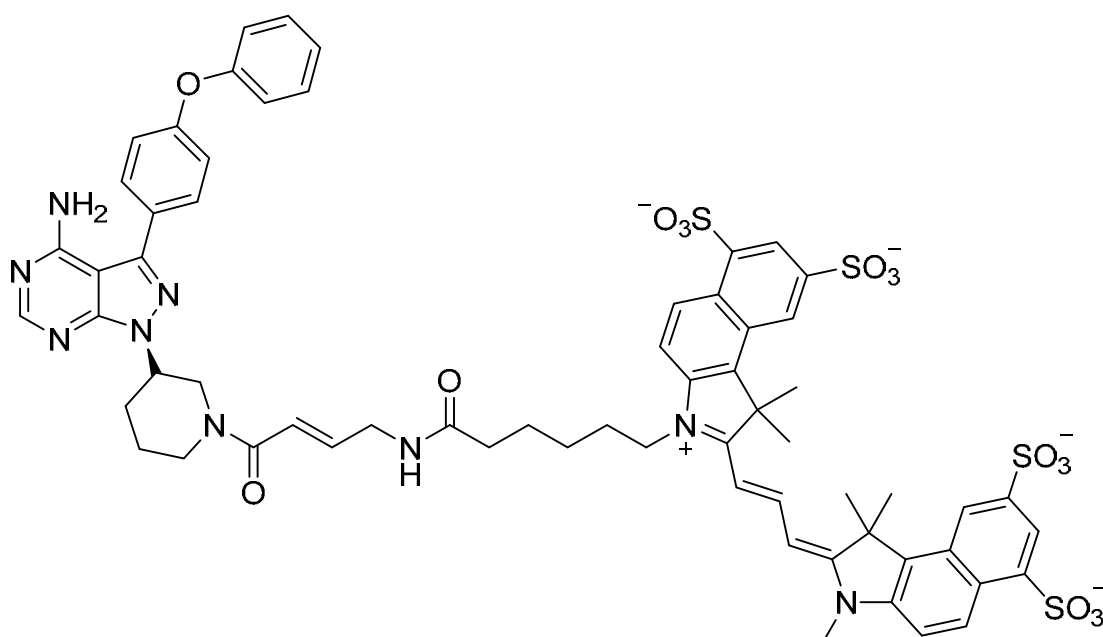


Ibrutinib derivative **9** (8.2 mg, 0.014 mmol, 1.05 eq.) was dissolved in dry DCM (0.5 mL) (dried over mol. sieves 4A), 4M solution of HCl(g) in dioxane (41.4 µL, 0.166 mmol, 12 eq.) was added and reaction mixture was stirred on room temperature until complete conversion of starting material (tracking by TLC[9]). Reaction mixture was evaporated with heating on 35°C. Residual white solid was dissolved in anhydrous DMF (0.5 mL) and NHS-ester of sulfo-cyanine3.5 dye (15 mg, 0.014 mmol, 1.0 eq.) dissolved in anhydrous DMF (0.5 mL) and DIPEA (72.0 µL, 0.414 mmol, 30 eq.) were added. Reaction mixture was stirred protected from light on room temperature until the

---

[9]  TLC (silica, 10% MeOH / EtOAc, det.: UV254nm & ninhydrin staining)

completion of the reaction (tracking by TLC[10]) and then was evaporated with heating on 35°C. Residue was triturated with pentane, $Et_2O$ and EtOAc, and after that was dried under high vacuum at room temperature to give 21 mg of crude product **ibrutinib-Cy3.5** in form of violet solid.

Analytically pure sample was prepared by SPE purification of crude product **ibrutinib-Cy3.5** on 12g $C_{18}$-RP flash cartridge. The cartridge was preconditioned by washing with water (10 mL). Crude product **ibrutinib-Cy3.5** (10 mg, 0.007 mmol) was dissolved in water (0.5 mL) and loaded on the cartridge. After that, the cartridge was washed with water (10 mL) and further with acetonitrile (10 mL) to remove impurities and side products of the reaction. Compound **ibrutinib-Cy3.5** was eluted with mixture ACN / $H_2O$ 1:1 (v/v) in a few fractions containing exclusively pure product. Collected eluates with the product were combined and lyophilised to give 8 mg of pure final product **ibrutinib-Cy3.5** (0.006 mmol, 80%) as violet solid.

TLC (RP-$C_{18}$, MeOH / $H_2O$ / AcOH 10:0.5:0.2 v/v/v, det.: UV/Vis & ninhydrin): $R_f$ = 0.90 (violet spot)

HPLC (RP-$C_{18}$, $CH_3CN/H_2O$): >95%

HRMS (ESI, neg): HRMS (ESI, $CH_3CN/H_2O$):

m/z calc. for $C_{64} H_{62} N_9 O_{15} S_4^{3-}$ [M-H] ($z$=3): 441.44216; found: 441.44160;

m/z calc. for $C_{64} H_{62} N_9 O_{15} S_4 H^{2-}$ [M-H] ($z$=2): 662.66687; found: 662.66630;

m/z calc. for $(C_{64} H_{62} N_9 O_{15} S_4 H)_2^{4-}$ [M-H] ($z$=4): 662.66687; found: 662.66630.

---

[10]  TLC (RP-$C_{18}$, MeOH / $H_2O$ / AcOH 10:0.5:0.2 v/v/v, det.: UV/Vis & ninhydrin staining)

**Supporting Figure 1: A**: High resolution mass spectrometry of Cy3.5-ibrutinib, **B**: HPLC-analysis of the final compound to ensure purity. Method: Mobile phase A = $H_2O$ + 0.1% TFA, Mobile phase B = $CH_3CN$ + 0.1% TFA, Column: Eurospher II 100-10 $C_{18}$, 250 x 4 mm, Flow = 3 mL / min, Detector: DAD (210 – 780 nm), λ1 = 254 nm, λ2 = 590 nm. Gradient: 0 min - 90% A; 2 min - 90% A; 12 min - 5% A; 15 min - 5% A; 18 min - 90% A.

**B**

λ=590nm

λ=254nm
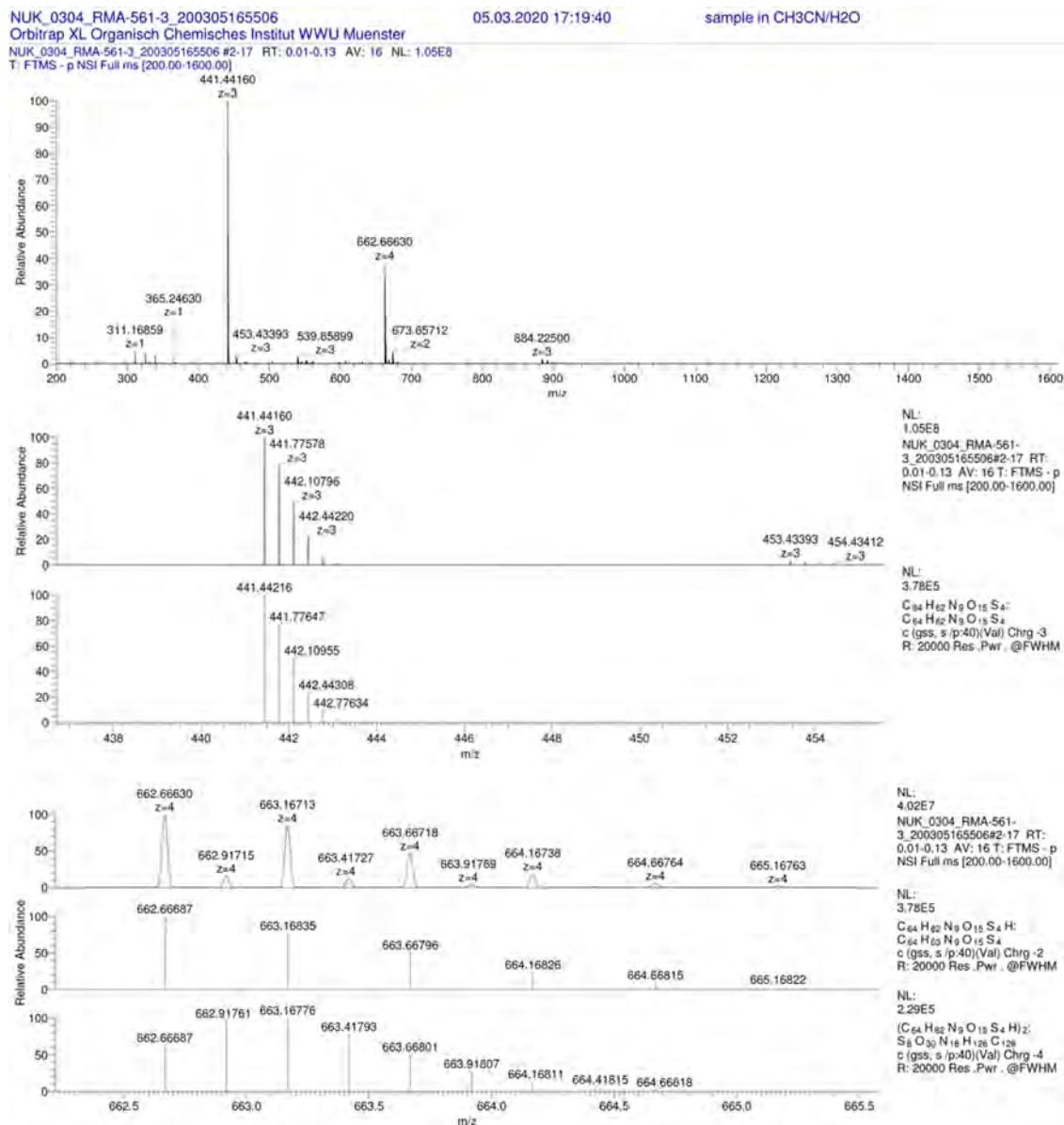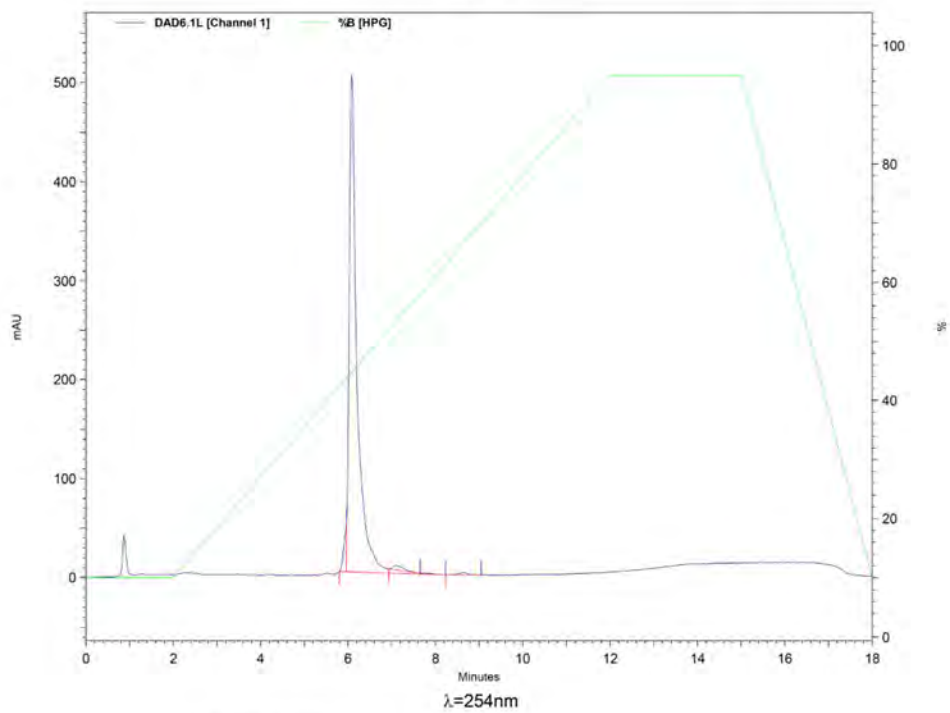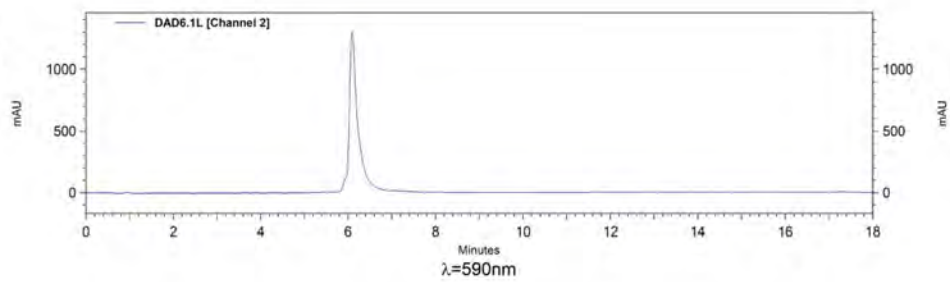
DAD6.1L [Channel 1]
Results

| Retention Time | Area | Area % |
|---|---|---|
| 5,950 | 194740 | 2,94 |
| 6,083 | 6318360 | 95,40 |
| 7,100 | 74847 | 1,13 |
| 8,650 | 35130 | 0,53 |

| Totals | | |
|---|---|---|
| | 6623077 | 100,00 |

## 2. Nanocarrier formation

### 2.1. Coupling of anti-CD20-mAB rituximab to protamine-sulfate

Coupling of the anti-CD20-mAB rituximab (Truxima®, Mundipharma) (αCD20-mAB) to protamine-sulfate was performed in a two-step synthesis (see Fig. 2 A). First, the positive charged protamine-sulfate (cat. No. 110123, Merck) was amino-terminally coupled to the bifunctional crosslinker sulfo-SMCC (Sulfosuccinimidyl 4-(N-maleimidomethyl) cyclohexane-1-carboxylate, cat.no. 13415-1, CovaChem,Loves Park IL, USA) at a molar ratio of 1:5 in ddH$_2$O. pH was adjusted to pH 6.0 wit 0.1 M carbonate buffer (pH 8.3). After incubation for 1 hour at 37°C uncoupled sulfo-SMCC was removed by gel filtration chromatography in Zeba spin desalting columns (Pierce No. 89891). Then, the sulfo-SMCC-protamine-complex was then coupled to cysteine residues of rituximab in a 32:1 molar ratio according to protamine-sulfate. The mixture was left to react over night at 4°C. Rituximab-protamine conjugates, here referred to as αCD20-mAB/P) were stored at 4°C and stable for several weeks.

### 2.2. Ibrutinib-Cy3.5 and rituximab-protamine/protamine (αCD20-mAB/P/P) complex formation

Negative charged ibrutinib-Cy3.5 was bound in 20 times molar excess to αCD20-mAB/P with free protamine present, if not stated otherwise, for ibrutinib at room temperature in the dark for 30-60 min. Complexes were prepared freshly before use.

### 2.3. Determination of ibrutinib-Cy3.5 load capacity

For the electromobility shift assay, a constant concentration of ibrutinib-Cy3.5 (15 µM) was incubated as described above with a decreasing amount of αCD20-mAB/P/P complexes from 10-fold up to 100-fold molar excess according to ibrutinib-Cy3.5. After incubation, the mixture was subjected to a 2% agarose gel electrophoresis stained with Red Safe.

### 2.4. Nanoparticle formation

For the analysis of *in vitro*-formation of nanoparticles, 1,200 nM ibrutinib-Cy3.5 was complexed in 60 nM αCD20-mAB/P (= 1:20 molar ratio) and free protamine as described above in a final volume of 200 µl PBS, RPMI medium with 10% FCS, or 50% FCS in PBS, respectively, and incubated in chamber slide (cat.no. 94.6140.202,

Sarstedt) over night at 37°C. The slides were then washed with PBS, fixed with cold 4% PFA, mounted with mounting medium (cat.no. 10121691, Dako North America) and analysed via fluorescence using a Nikon Eclipse 50i upright microscope.

## 3. *In vitro* evaluation

### 3.1. Cell culture

Human DLBCL cell line HBL1 was maintained in RPMI-1640 medium (cat.no. 21875-034, Thermo Fisher) supplemented with 10% fetal bovine serum (FBS) and 1% streptomycin and penicillin. Human DLBCL cell line TMD8 was cultivated in IMDM medium (cat.no. 21980-032, Thermo Fisher) supplemented with 10% FBS, 1% sodium pyruvate and 1% penicillin and streptomycin. Both cell lines were cultivated at a cell density of $0.2 - 1 \times 10^6$ cells/ml and incubated at 37°C with 5% $CO_2$ in high humidity.

### 3.2. Flow cytometry

To approve the internalisation of the αCD20-mAB/P/P complexes with ibrutinib-Cy3.5, cells were treated over night with 60 nM αCD20-mAB/P/P, 60 nM uncoupled αCD20-mAB, or PBS, respectively. Cells were washed with PBS and analysed by flow cytometry using a BD FACSCalibur.

### 3.3. Fluorescence microscopy

Cell lines were seeded at $2 \times 10^5$ cells/ml and treated with PBS, 60 nM αCD20-mAB/P/P complexed with 1,200 nM ibrutinib-Cy3.5, or 1,200 nM uncomplexed ibrutinib-Cy3.5 overnight at 37°C and 5% $CO_2$. For BTK occupancy analysis, HBL-1 cells were treated with PBS, 2,400 nM ibrutinib-Bodipy-FL (PCI-33380, cat. no. HY-100335, Hölzel-Diagnostika, Cologne, Germany) or 2,400 nM ibrutinib for 2 h, washed with medium and treated for 4 h or 24 h with 120 nM αCD20-mAB/P/P complexed with 2,400 nM ibrutinib-Cy3.5.

Cells were washed twice with cold PBS, transferred to adhesion slides (ImmunoSelect Adhesion Slides, cat.no. SQ-IS-10100, MoBiTec) bordered with a liquid blocker pen. Cells were incubated on ice for 20 minutes to stick to surface, fixed with ice-cold 4% paraformaldehyde (PFA), stained with Hoechst33342 (cat.no. H1399, Thermo Fisher),

mounted with mounting medium (cat.no. 10121691, Dako, Santa Clara, CA, USA). Slides were photographed on a Nikon Eclipse 50i upright microscope or on a Keyence BZ 9000 (Figure 2).


## 3.4. Electron microscopy

Freshly prepared nanoparticles were sedimented on an formvar-coated, carbon-sputtered copper grid. After negative staining with 1% phosphotungstic acid, pH 7, the samples were analyzed at 80kV on a Tecnai 12 electron microscope (Fei, Eindhoven, The Netherlands). Images of selected areas were documented with Veleta 4k CCD camera (Emsis, Münster, Germany).

## 3.5. Apoptosis assay

To determine apoptosis, cells were treated with uncoupled rituximab, ibrutinib-Cy3.5, free ibrutinib (Imbruvica$^R$) and or αCD20-mAB/P/P-ibrutinib-Cy3.5 at a final concentration of 60nM relating to rituximab and 1200nM relating to ibrutinib. Treatments were repeated twice at consecutive days. After 72 h, cells were stained for AnnexinV expression (APC AnnexinV, cat.no. 550474, BD Pharmingen) and analysed by flow cytometry.

## 3.6. Colony formation assays

For HBL1 colony formation, 2,500 cells were seeded in 150 µl culture medium per sample. Cells were incubated with different conditions of αCD20-mAB/P/P (60 nM) coupled in a 1:20 molar ratio to ibrutinib-Cy3.5 in a final volume of 750 µl for at least two hours at 37°C. Afterwards, cell suspension was mixed with 600 µl methylcellulose M3231 (cat. No. 03231, Stemcell Technologies) and seeded in triplicates for colony formation in 96-well format (150 µl/well). For TMD8 colony formation, 2,000 cells were seeded in 150 µl culture medium per sample. Cells were treated with αCD20-mAB/P/P-complexes coupled and incubated as described above. Then, 432 µl culture medium and 168 µl 2% agar (agar noble, cat.no. 214220, BD) was added and mixture was also divided in triplicates in 96-well format (180 µl/well). After 5-7 days, the assays were stained with 20 µL 4 mg/ml iodonitrotetrazolium chloride (INT) solution and incubated overnight at 37°C. The assays were counted for colony numbers using a binocular.

## 3.7. SDS-Page and Western blot

$2\times10^5$ cells each cell line were seeded and treated over night with ibrutinib-Cy3.5 or αCD20-mAB/P/P-ibrutinib Cy3.5. Cells were harvested after 24, 48 or 72 hours, washed with PBS and resuspended directly in NuPage™ SDS sample buffer (cat.no. NP0007, Invitrogen) supplemented with 1x NuPage™ Sample reducing agent (cat.no. NP0004, Invitrogen, Thermo Fisher), boiled for 5 minutes at 95°C, applied to a 10% SDS-PAGE. Before blotting, gel was photographed with Intas ECL Chemostar Imager. Western blot analysis was performed using standard procedures. Analyses were performed using following antibodies: anti-BTK (Cell Signaling #3532), anti Phospho-BTK-Tyr223 (Cell Signaling, #5082), anti-phospho-ERK (Cell Signaling, #4370), anti-total-ERK (Cell Signaling, #4696) and anti-β-Actin (Clone AC-15, Sigma Aldrich).


## 4. *In vivo* evaluation

All animal experiments in this study were carried out in accordance with the recommendations of the Institutional Animal Care and Use Committee "Landesamt fuer Natur, Umwelt und Verbraucherschutz NRW" (LANUV). This study was performed with permission of the Institutional Animal Care and Use Committee and of the local veterinary administration of Münster (Permit no. 81-02.04.2017.A439).

### 4.1. Mouse xenograft tumor model

$1\times10^7$ HBL1 cells resuspended in 1:1 PBS and matrigel were injected subcutaneously in the flank of 50 NSG-mice. When tumors reached a measurably size of at least 150 mm³ mice were randomized divided into treatment groups.

αCD20-mAB-protamine (calculated for the mAB) and unmodified αCD20-mAB antibody were applied intra-peritoneal, twice a week at 4 mg antibody/kg mouse weight in the first experimental line, which equals a 120 µg or 0.75 nmol single dose for a 30 g mouse. This was complexed before in a 1:20 molar ratio to ibrutinib-Cy3.5, which leads to 15 nmol single dose of ibrutinib-Cy3.5. As a control, un-complexed ibrutinib-Cy3.5 was given in the same dose. In the second line of *in vivo* experiments, all doses were doubled. Uncharged ibrutinib (cat.no. HY-10997, MedChem-Express) was

applied at 15 nmol single dose in the same routine as above. Mouse weight was determined before each treatment.

Tumor growth was measured with a caliper and tumor volume was calculated by the formula length x width² x 0.52. When the tumor volume reached an intolerable size >1,500 mm³, the respective mouse was euthanized, tumor, spleen, liver, lung, sternum, femur, heart and kidney were isolated and prepared for further analysis and serum was prepared from blood samples for determination of liver enzyme activity of GOT (glutamate-oxalacetate-transaminase) and GPT (glutamate-pyruvate-transaminase) using standard procedures. The survival was statistically evaluated in a Kaplan-Meier plot. For the second trial, double amount of αCD20-mAB/P was tested (8 mg/kg αCD20-mAB/P, 1.44 mg/kg ibrutinib).

## 4.2. *Ex vivo* fluorescence imaging (biodistribution)

Excised organs and tumors were placed at a petri dish and imaged in a Fluorescence Reflectance Imager (*in vivo* MS FX Pro, Bruker Biospin MRI GmbH, Ettlingen, Germany). First, a white light image was taken, followed by a fluorescence image with an exposure time of 30 sec. The fluorescent protein was excited with light at a wavelength of 530 nm (±10 nm) and fluorescence was registered within the wavelength of 600 nm (± 17,5 nm). The data was analysed with the imaging software MISE (Bruker, v 7.5.2).

**Supporting Figure 2: Properties of the αCD20-mAB-protamine. A:** Flow cytometric analysis HBL1 cells stained for CD20 surface expression. When cells were incubated with αCD20-mAB-P/P, the CD20-receptor disappears from the cell surface. Dark grey curve: CD20-expression on untreated cells (positive control), light grey: incubation with unconjugated αCD20-mAB, green: incubation with αCD20-mAB-protamine (-P); black: unstained cells (negative control). FACS staining was performed with a labelled anti-CD20 antibody binding a separate epitope from the one bound by the targeting anti-CD20 antibody used. **B:** electromobility shift assays showing the electrostatic loading capacity of ibrutinib-Cy3.5 to conjugates.
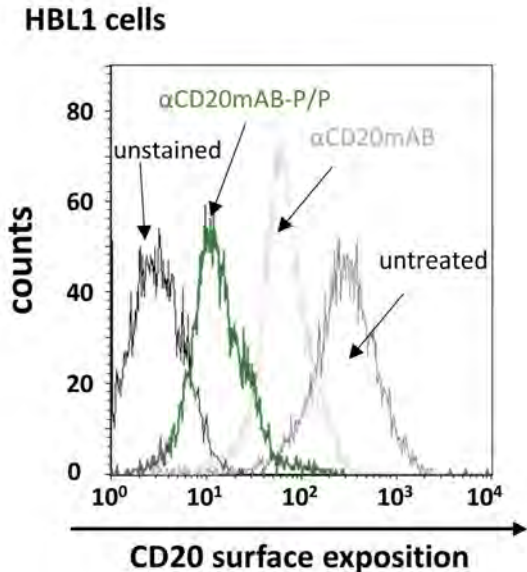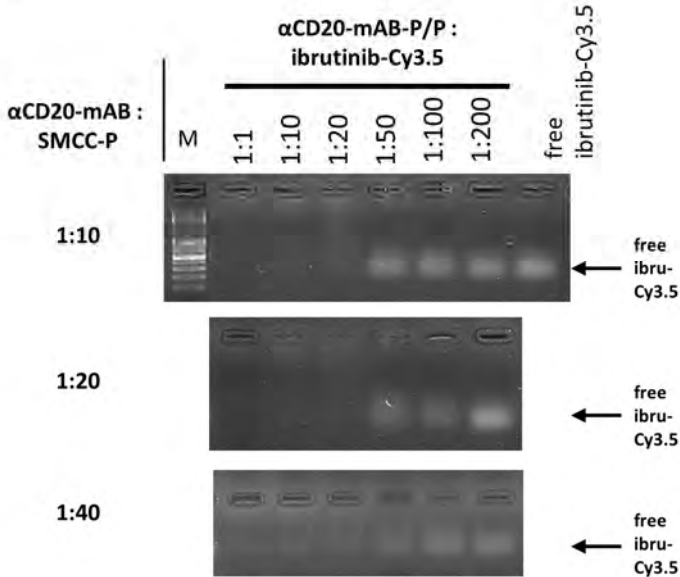
**Supporting Figure 3**: **A:** Affinity chromatographic purification (HPLC) of the αCD20-mAB-protamine conjugate. αCD20-mAB-protamine conjugation mix was applied to protein G sepharose column equilibrated with PBS and eluted with buffer pH 2.5. Elution fractions were collected and subjected to SDS-PAGE and Coomassie stain. The last fractions 25/26 contained αCD20-mAB-protamine conjugate purified from excess free SMCC-protamine, which was used in further analysis. **B:** The SMCC-protamine purified fraction 25 conjugate (left; "after HPLC") was compared to the input control with free SMCC-protamine (right) in terms of ibrutinib-Cy3.5 complexation ability. Whereas the input control with free SMCC-protamine was able to complex ibrutinib-Cy3.5 in all tested conditions, the variant purified from free SMCC-protamine showed no distinct binding affinity to ibrutinib-Cy3.5.
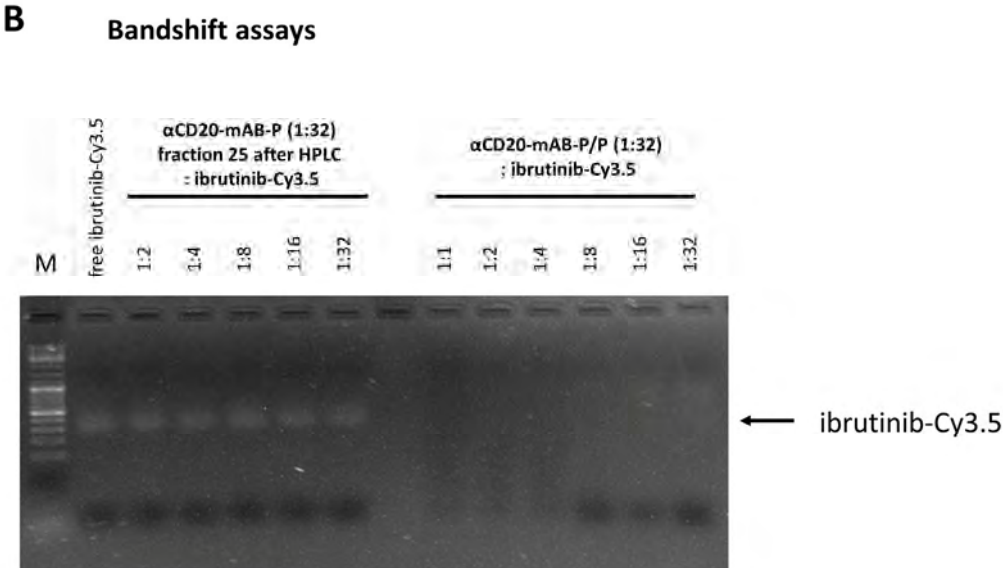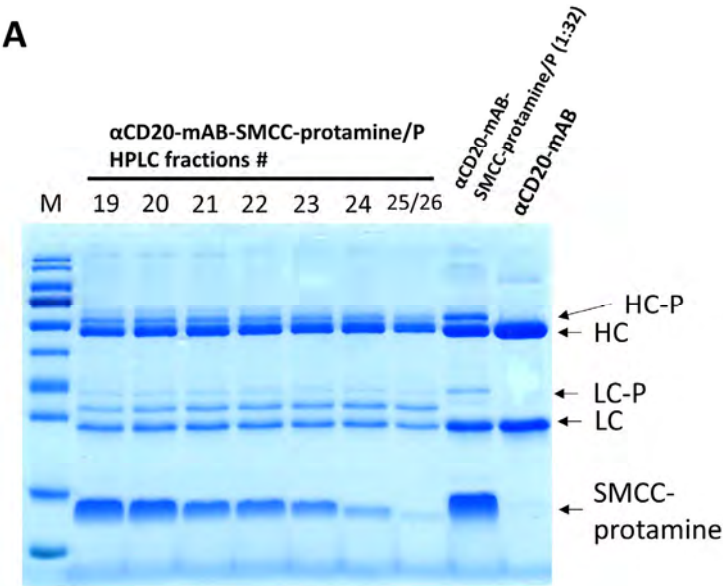
**Supporting Figure 4: Cellular targeting of Bruton's kinase BTK by αCD20-mAB-P/P loaded ibrutinib-Cy3.5. A-F:** Fluorescence microscopy of TMD8 DLBCL cells treated with targeted nanocarriers and controls showing a marked intracellular enrichment of Cy3.5-signals upon the incubation with αCD20-mAB-P/P loaded ibrutinib-Cy3.5. **G-H:** Lysates from cells treated for 24 h (G) and 48 h (H) with targeted nanocarriers and controls were subjected to SDS PAGE and illuminated for Cy3.5 signals. A clear band of 70 kDa, identified as BTK by parallel immunoblot was covalently marked by ibrutinib-Cy3.5, indicating binding and functionality of the ibrutinib-Cy3.5 derivate. tBTK, total BTK.
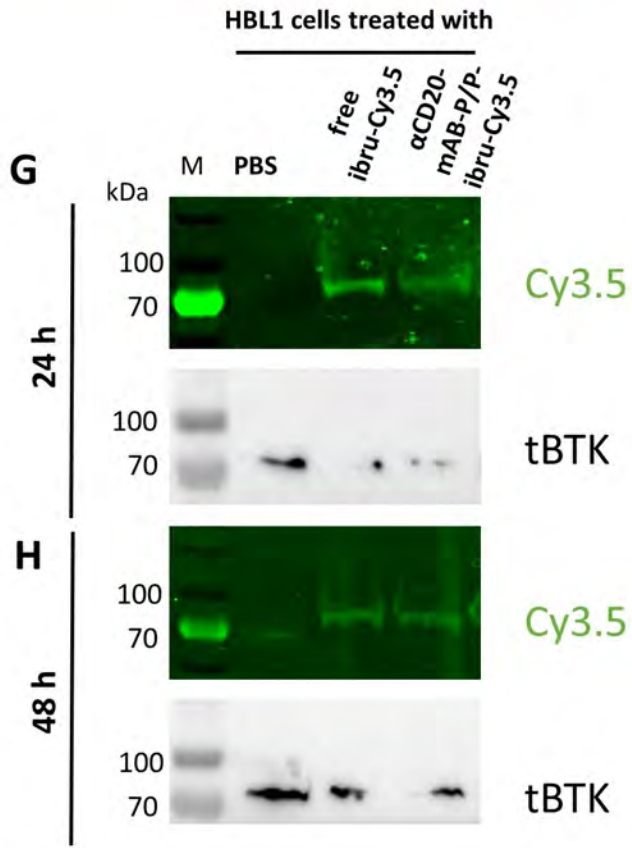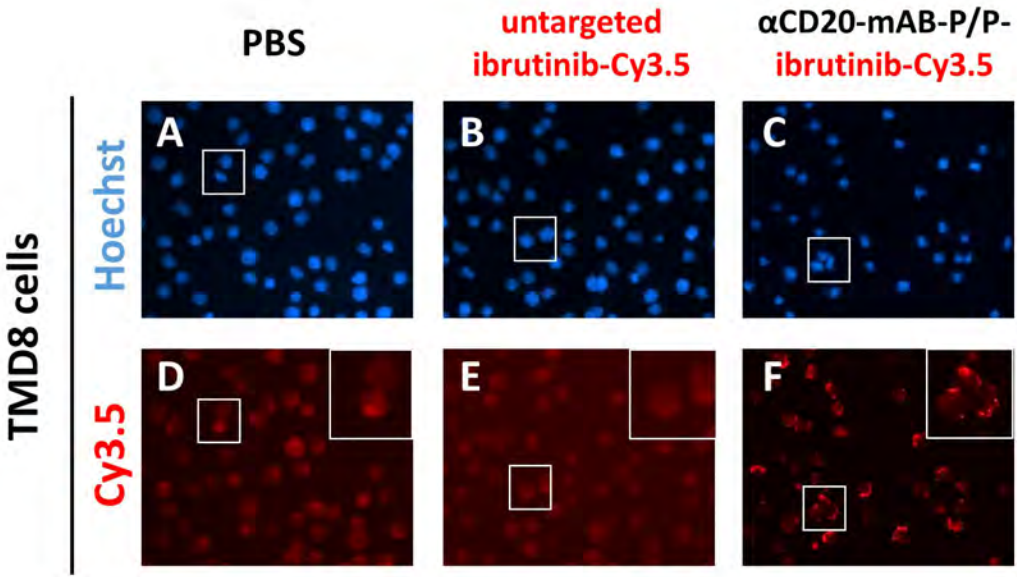
**Supporting Figure 5: A-I.** Fluorescence microscopy of HBL1 DLBCL cells pre-treated with ibrutinib-bodipy (green, G and I) do not show intracellular enrichment of Cy3.5-signals after αCD20-mAB-P/P-ibrutinib-Cy3.5 treatment (F, compared to E).
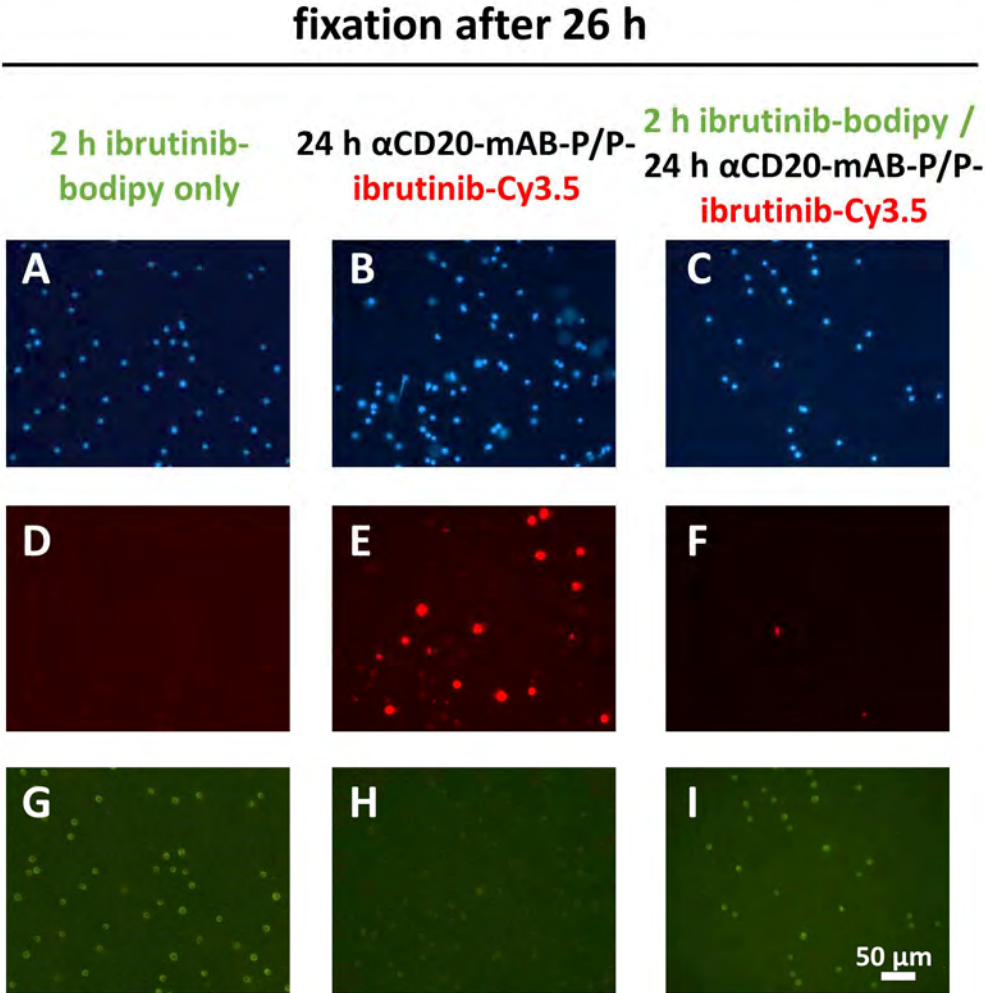
**Supporting Figure 6: A-F.** Fluorescence microscopy of HBL1 DLBCL cells pre-treated with ibrutinib (**G** and **I**) do not show intracellular enrichment of Cy3.5-signals after αCD20-mAB-P/P-ibrutinib-Cy3.5 treatment (**F**, compared to **E**).
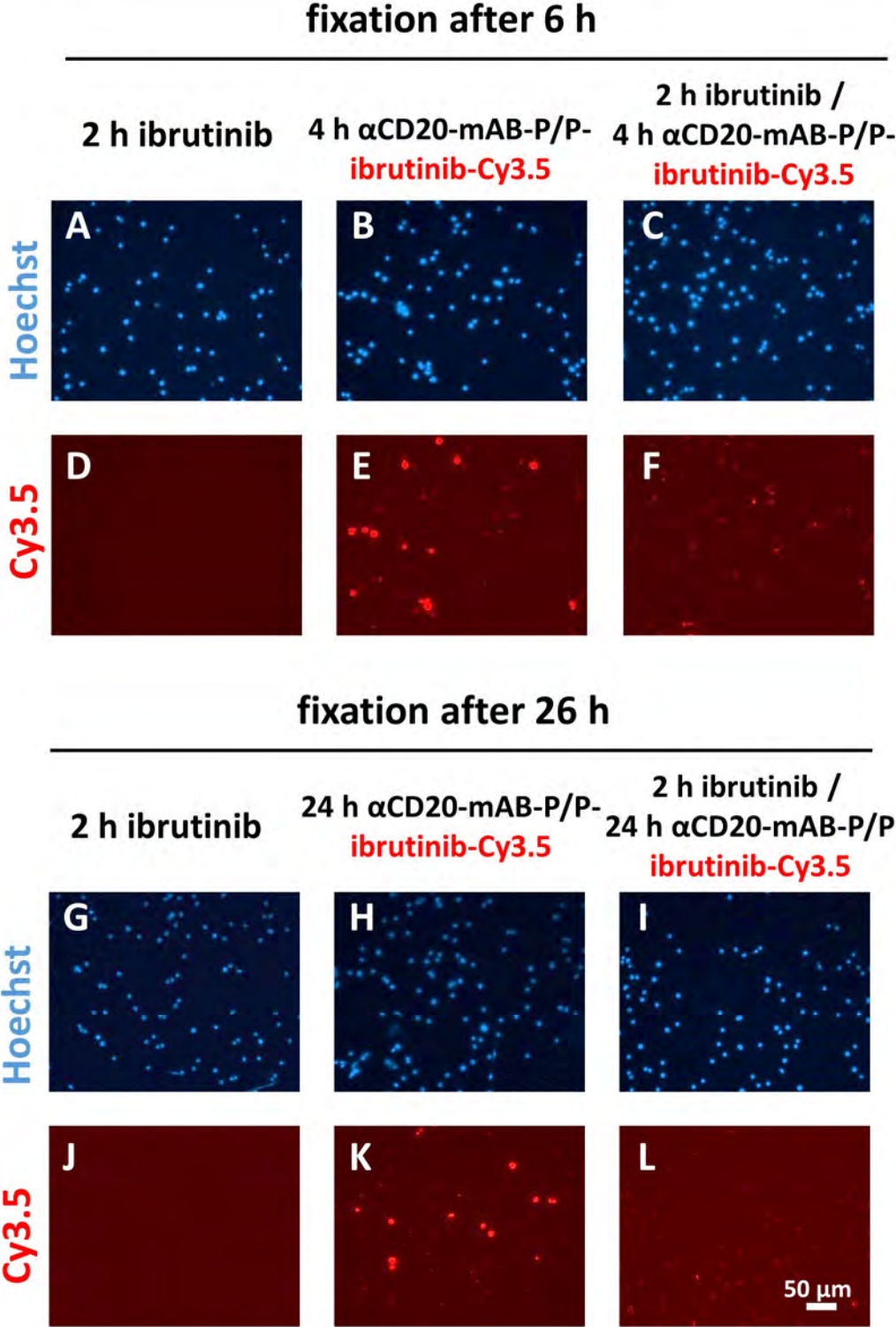
**Supporting Figure 7: Physiological and functional consequences of BTK-inactivation by αCD20-mAB-P/P-ibrutinib-Cy3.5 nanocarrier treatment in DLBCL cell lines. A**: TMD8 cells were treated by the respective conjugates shown for 72 hrs, lysed and subjected to SDS-PAGE and Western blotting for phospho-BTK (pBTK), total BTK (tBTK), phospho-ERK (p-ERK), total-ERK (t-ERK) and actin as a loading control. Free ibrutinib-Cy3.5 inhibited the phosphorylation of BTK a bit less than αCD20-mAB-P/P-ibrutinib-Cy3.5 nanocarrier. The difference of expected downstream phosphorylation targets such as ERK was more pronounced: Only αCD20-mAB-P/P-ibrutinib-Cy3.5 treatment was able to reduce ERK phosphorylation significantly. **B:** In colony formation assays, targeted αCD20-mAB-P/P/ibrutinib-Cy3.5 strongly reduced colony growth of TMD8 cells.
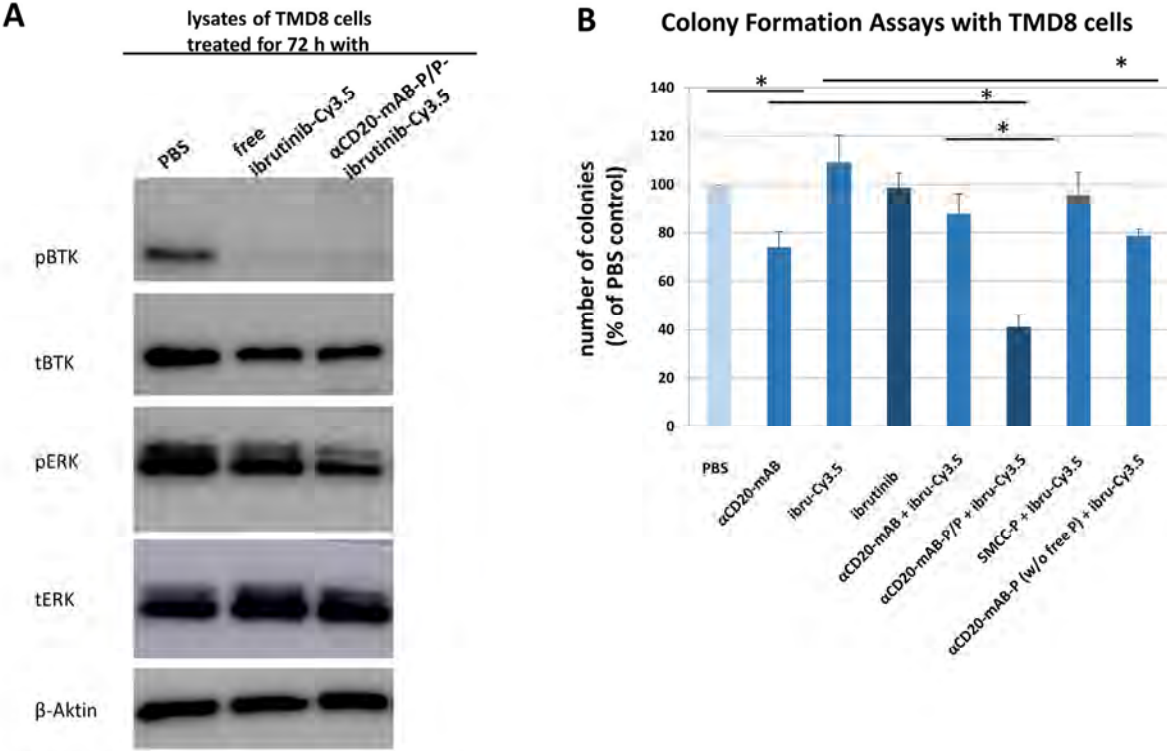
**Supporting Figure 8: Induction of apoptosis of BTK targeting by αCD20-mAB-P/P-ibrutinib-Cy3.5 nanocarrier treatment in DLBCL cell lines.** TMD8 cells were treated by the respective conjugates shown for 72 hrs and subjected to AnnexinV-staining. Apoptotic cells were detected by AnnexinV-expression (X-axis) by flow cytometry (upper panels), while Cy3.5-dependend fluorescence was detected on the Y-axis. Values from upper right and lower right gates were counted. Lower panel: AnnexinV-positive cells in three independent experiments were summarized. P<0.05, 2-sided T-test.
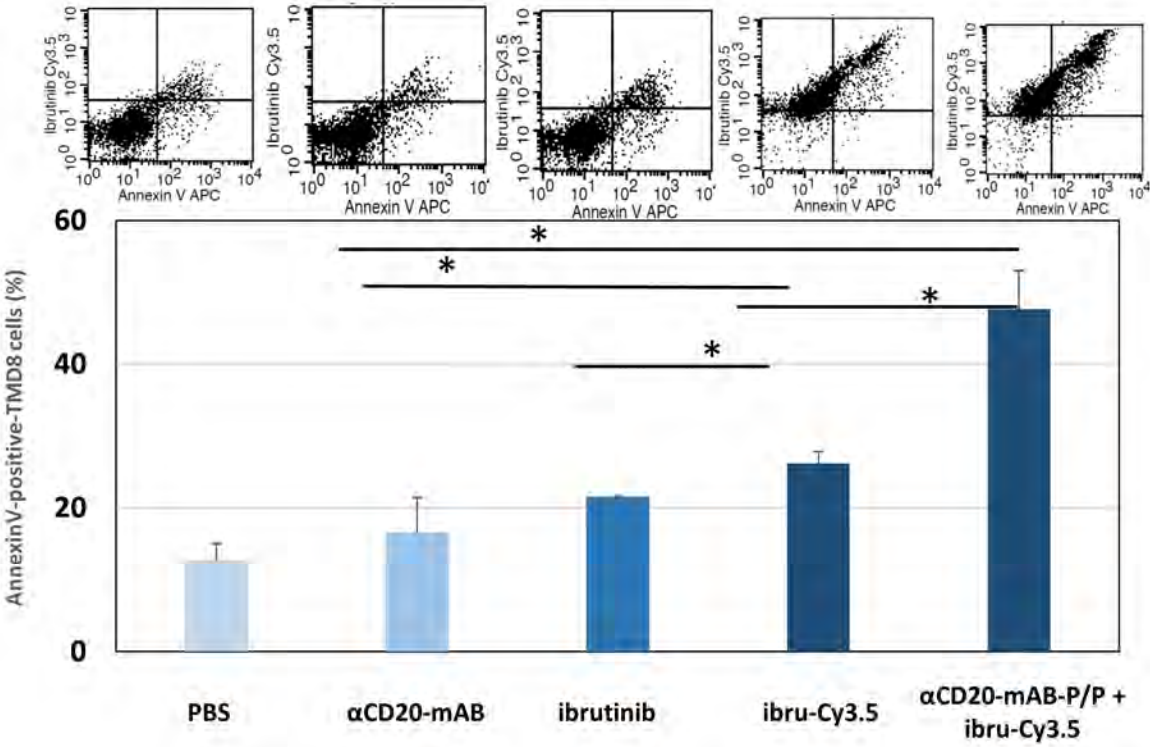
**Supporting Figure 9: Determination of toxicity parameters in transplanted and treated mice. A:** In the *in vivo* experimental trial presented in Figure 6 A (4 mg/kg), mouse weight values were determined on day one and after the treatment on day 11. The values varied insignificantly in all groups exposing no obvious signs of toxicity. **B:** Blood plasma was withdrawn from mice on the day of treatment termination and subjected to test for clinical liver parameters GOT glutamate-oxalacetate-transaminase) and GPT (glutamate-pyruvate-transaminase). Here, the values clearly differed and showed that αCD20-mAB-P/P-ibrutinib-Cy3.5 treated mice exposed GOT values comparable to PBS and antibody control groups, whereas the untargeted compounds showed significantly elevated GOT values. A similar picture is seen, when GPT plasma values of αCD20-mAB-P/P-ibrutinib-Cy3.5 treated mice are compared to untargeted ibrutinib and ibrutinib-Cy3.5: Also here, GPT levels was significantly lower in the complex treatments vs ibrutinib-treatment. **C:** Here, mouse weights for the *in vivo*-trial presented in Figure 6 B (8 mg/kg) are determined with no significant differences in the treatment groups. GOT/GPT liver parameters have not been recorded in this trial. P<0.05, 2-sided T-test.